Journal of Controlled Release 389 (2026) 114411

Contents lists available at ScienceDirect

Journal of Controlled Release

journal homepage: www.elsevier.com/locate/jconrel

An antioxidant metal-organic framework with functional coatings for oral anti-TNF-α antibody delivery in inflammatory bowel disease treatment

Cheng Chen [a], Léo Guilbaud [a], Valentina Marotti [a], Wunan Zhang [a], Inês Domingues [a], Hafsa Yagoubi [a], Katlijn Vints [b], Yining Xu [c,*], Ana Beloqui [a,d,*]

[a] UCLouvain, Université catholique de Louvain, Louvain Drug Research Institute, Advanced Drug Delivery and Biomaterials, 1200 Brussels, Belgium
[b] EM-platform, VIB Bio Imaging Core, KU Leuven, Campus Gasthuisberg, Herestraat 49, 3000 Leuven, Belgium
[c] Department of Pharmacy, Institute of Metabolic Diseases and Pharmacotherapy, West China Hospital, Sichuan University, Chengdu 610041, China
[d] WEL Research Institute, avenue Pasteur, 6, 1300 Wavre, Belgium

ARTICLE INFO

Keywords:
Oral biomacromolecule delivery
Oral antibody
Metal-organic framework
Anti-inflammatory treatment
Inflammatory bowel disease

ABSTRACT

Oral biomacromolecule delivery is considered a promising alternative for patients who must receive long-term invasive injections, providing better patient compliance. However, it still faces great challenges due to the harsh gastrointestinal environment, including instability and poor intestinal absorption. Here, we report an antioxidant moiety (manganese ion, Mn^{4+})-assembled metal–organic framework (MOF) presenting functionalized coatings consisting of an inner layer of hyaluronic acid–polyethylene glycol and an outer layer of Eudragit® S100 for enhanced colon-targeted delivery of an anti-mouse tumor necrosis factor-alpha (TNF-α) antibody *via* oral route. The developed anti-TNF-α antibody-MOF system presented gastric resistance, enhanced targeting of the inflamed intestine, and antioxidant activity. In acute inflammatory bowel disease (IBD) models, the therapeutic effect of the oral anti-TNF-α antibody-MOF system was similar, or even better, than that of intravenous injections at the same antibody dose, with superior antioxidant and mucosal healing capacities. We also demonstrated that in a chronic murine colitis model, the oral anti-TNF-α antibody-MOF system significantly reduced the pathological features of the disease, especially the levels of proinflammatory factors and oxidation markers, which did not differ significantly from those in healthy mice. Overall, this study provides a promising strategy for the oral delivery of antibodies in IBD treatment.

1. Introduction

Oral biomacromolecule delivery is considered the preferred therapeutic strategy for patients with chronic gastrointestinal (GI) diseases, such as inflammatory bowel disease (IBD), who often receive invasive needle injections [1]. IBD, which includes ulcerative colitis (UC) and Crohn's disease (CD), is an autoimmune, relapsing–remitting chronic disease of the GI tract (GIT) whose prevalence has increased substantially worldwide and is becoming a public health threat [2]. Conventional IBD treatment includes aminosalicylates, corticosteroids, and immunomodulators, often accompanied by additional measures or surgical interventions [3]. The advent of biologic monoclonal antibody therapies has revolutionized IBD treatment, improving response and remission rates [4]. However, this class of biomacromolecule drugs, whose molecular weight can reach 150 kDa [5], requires repeated invasive parenteral administrations, causing severe systemic side effects and poor patient compliance [6]. Therefore, the development of delivery systems that can deliver antibody drugs to the site of intestinal inflammation *via* alternative delivery routes is needed.

Oral administration would represent a more convenient alternative for the delivery of biologic monoclonal antibody therapies in IBD since this route is painless, and can directly target the site of inflammation in the GIT [7]. Nevertheless, no biologic monoclonal antibody drug formulation has been approved for oral use owing to the multiple biological and physiological barriers at the GIT, often resulting in poor stability and low bioavailability [8]. These include harsh acidic conditions in the stomach, different proteolytic enzymes (such as pepsin, trypsin, and chymotrypsin), and thick and viscous mucus layers [9,10]. IBD is associated with dysfunction of the intestinal mucosal barrier, leading to the invasion of luminal contents into the gut mucosa and triggering hyperactive immune responses characterized by elevated levels of reactive oxygen species (ROS) and proinflammatory cytokines

* Corresponding authors.
E-mail addresses: yiningxu@scu.edu.cn (Y. Xu), ana.beloqui@uclouvain.be (A. Beloqui).

https://doi.org/10.1016/j.jconrel.2025.114411
Received 17 August 2025; Received in revised form 27 October 2025; Accepted 13 November 2025
Available online 14 November 2025

and chemokines [11]. Although injectable monoclonal antibodies targeting proinflammatory cytokines, such as anti-tumor necrosis factor-alpha (TNF-α) antibodies, have shown remarkable efficacy at alleviating IBD symptoms, there is still no cure for IBD [12]. Strategies targeting multiple pathological pathways involved in IBD have shown additional benefits for IBD treatment [13–15]. Furthermore, owing to the impact of the disease in the colon, colon-targeted oral drug delivery is an attractive strategy for IBD treatment [16]. The specific physiological and pathological characteristics of colon lesions in IBD patients represent promising targets, presenting enhanced permeability and retention at inflamed sites and the overexpression of certain receptors on activated macrophages (*e.g.*, cluster of differentiation 44, cluster of differentiation 98 or folate receptor) [17,18].

Various strategies, including enzyme inhibitors, permeation enhancers, and nanocarriers, have been explored to facilitate oral antibody delivery, with nanoparticle-based approaches showing particular promise [19–21]. However, the effectiveness of most of these nanoparticle-based strategies for the oral delivery of monoclonal antibody drugs is still limited and has not met the clinical needs [22–27]. Metal–organic frameworks (MOFs), consisting of organic ligands and metal ions/clusters *via* coordinative bonds and electrostatic interactions, are highly ordered, porous, and crystalline materials with protective effects on proteolysis. MOFs can be prepared by mild synthesis with biomacromolecules *via* biomineralization, and offer versatile surface functionalization [28], holding great potential for biomacromolecule delivery [29]. Furthermore, some metal ions possess inherent therapeutic activities; for example, manganese (Mn^{4+})-based nanozymes exhibit antioxidant effects, such as superoxide dismutase (SOD)-like, catalase (CAT)-like, and hydroxyl radical-scavenging effects, highlighting their potential as antioxidant therapy [30].

In this study, the antioxidant Mn^{4+} was integrated with the organic ligand 2-methylimidozole, enabling the successful loading of an anti-mouse TNF-α monoclonal antibody (mAb-MOF) with high encapsulation efficiency. The mAb-MOF was further functionalized with mucopenetration and inflammatory cell-targeting properties *via* a hyaluronic acid-polyethylene glycol (HA-PEG) coating (mAb-MHP) to maximize the benefits of anti-inflammatory biomacromolecules and ROS-scavenging agents against IBD [31,32]. Considering the potential advantages of local treatment, to enhance colonic targeting while minimizing systemic exposure [16], we further coated the mAb-MHP with the pH-sensitive polymer Eudragit® S100 (mAb-MHPE) for colon-specific release. Eudragit® S100 (ES100) remains nonionized under acidic conditions, avoiding the degradation of nanoparticles and drugs, and has been found to be released at the colonic site at a pH above 7 [16]. In summary, an antioxidant MOF coated with functional layers was engineered for oral colonic antibody delivery in IBD treatment (Scheme 1). To the best of our knowledge, no previous studies have reported MOF-based nanosystems capable of specifically targeting inflamed colon sites and alleviating IBD symptoms, while protecting antibodies and achieving therapeutic efficacy comparable to, or even better than, that of intravenous administration at the same dosage.

2. Materials and methods

2.1. Materials

An anti-mouse TNF-α antibody (mAb) was purchased from BioxCell (Lebanon, USA). 2-methylimidozole (2-MIM), manganese(II) chloride

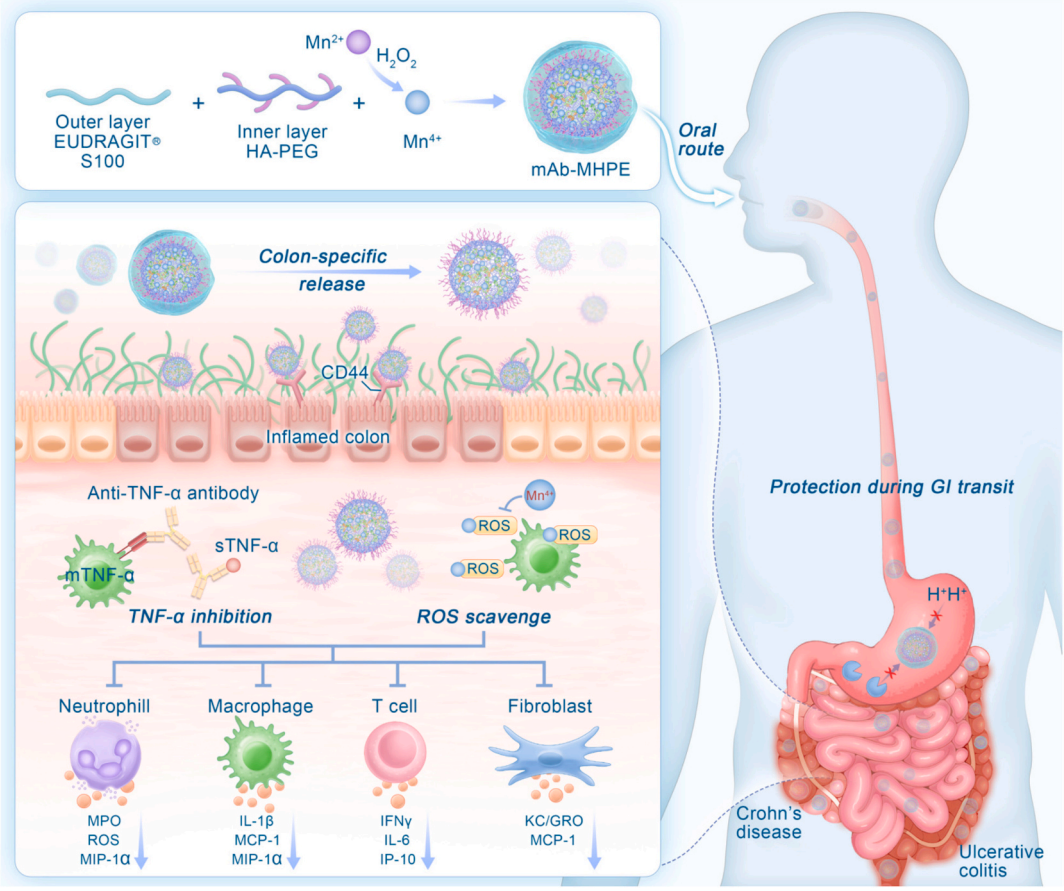

Scheme 1. Schematic illustration of an antioxidant MOF nanoparticle for enhanced oral anti-TNF-α antibody delivery to treat IBD. After oral administration, mAb-MHPE protected the loaded mAb during gastrointestinal (GI) transit and delivered mAb to the inflamed colon. It alleviated several pathological pathways involved in IBD by decreasing TNF-α levels and scavenging ROS.

tetrahydrate ($MnCl_2 \bullet 4H_2O$), hydrogen peroxide (H_2O_2), sodium bicarbonate ($NaHCO_3$), sodium carbonate (Na_2CO_3), sodium azide (NaN_3), Tween® 20, dimethyl sulfoxide (DMSO), sodium taurocholate, sodium chloride, polyvinyl alcohol, 3-(4,5-dimethylthiazolyl-2)-2,5-diphenyltetrazolium bromide (MTT), 2,4,6-trinitrobenzenesulfonic acid (TNBS), hexadecyltrimethylammonium bromide (HTAB), cetyltrimethylammonium bromide (CTAB), barium iodide, lipopolysaccharides (LPS) from *Escherichia coli O26:B6,* and polyvinyl alcohol (PVA) were purchased from Sigma-Aldrich (St. Louis, USA). 1-Step™ Ultra TMB-ELISA, RPMI-1640 medium, and Dulbecco's phosphate-buffered saline (DPBS) were purchased from Thermo Fisher Scientific (Massachusetts, USA). Eudragit® S100 (ES100) was kindly provided by Evonik Operations GmbH (North Rhine-Westphalia, Germany). TRIzol and ELISA assay buffer were purchased from Invitrogen (Massachusetts, USA). Sodium hyaluronate (Mw 1 MDa) was purchased from Lifecore Biomedical LLC (Chaska, MN, USA). PEGylated hyaluronic acid (Mw HA 1mDa and PEG 2 kDa) was purchased from Creative PEGWorks (North Carolina, USA). DSPE-PEG (Mw 2 kDa) was purchased from Nanosoft Polymers (NC, USA). Protease inhibitor cocktail tablets (cOmplete mini, EDTA free) were purchased from Roche Diagnostics (Vilvoorde, BE). Triton X-100 was purchased from Carl Roth (GmbH, DE). Sodium dodecyl sulfate (SDS) was purchased from Bio-Rad (BE). Dextran sulfate sodium (DSS, Mw ~40 kDa) was purchased from TdB Consultancy (Uppsala, SE). Mouse TNF-α ELISA kits and V-PLEX Custom Mouse Biomarkers ELISA kits were purchased from Meso Scale Discovery (Maryland, USA). The primers used within the manuscript were purchased from Integrated DNA Technologies (Lowa, USA). FaSSIF-V2 powder and FaSSCF powder were purchased from Biorelevant (London, UK). All chemical reagents utilized in this study were of analytical grade.

2.2. Preparation and characterization of mAb-MOF

The mAb-MOF was prepared by mixing 500 μL of the mAb (1 mg/mL) with 250 μL of 2-MIM (13 mg/mL) and incubating the mixture for 10 min. Subsequently, 250 μL of $MnCl_2 \bullet 4H_2O$ (7.9 mg/mL) was added to the mixture, followed by the addition of 50 μL of H_2O_2 (3.7 mg/mL) under vigorous stirring. The mAb-MOF was then obtained by centrifugation (VWR® Mega Star 1.6R, USA) at 7000 x *g* for 10 min. The encapsulation efficiency of the mAb was determined using a Bradford protein assay kit (Thermo Scientific, USA), and the encapsulation efficiency of Mn was assessed by inductively coupled plasma atomic emission spectroscopy (ICP-AES). X-ray photoelectron spectroscopy was employed to analyze the chemical valence of Mn [33].

2.3. Competitive ELISA

The activity of the loaded mAb was evaluated *via* a competitive ELISA, as described by Zhang *et al.* [34]. TNF-α was dissolved in a coating buffer containing 1.59 mg/mL $NaHCO_3$, 2.94 mg/mL Na_2CO_3, and 0.5 mg/mL NaN_3. A volume of 100 μL of this solution was added to each well of a 96-well plate and incubated overnight at 4 °C. The plate was then washed three times with 0.05 % (*v*/v) Tween® 20 and blocked with ELISAPOT for 2 h. Serial dilutions of mAb and mAb-MOF solutions (ranging from 40 μg/mL to 0.31 μg/mL) were prepared, and 50 μL of each diluted sample was mixed with 50 μL of biotin-labeled mAb (660 ng/mL). The resulting 100 μL mixture was incubated in the wells for 2 h at room temperature. Following incubation, the wells were washed three times and 100 μL of streptavidin–horseradish peroxidase (20 ng/mL in ELISA buffer) was added, followed by a 45-min incubation at 37 °C. The wells were subsequently washed six times, and 100 μL of TMB solution was added. After a 15-min incubation, 100 μL of 1 M phosphoric acid was added to stop the reaction. Absorbance was measured at 450 nm using a SpectraMax® plate reader (Molecular Devices, USA).

2.4. Preparation and characterization of mAb-MHP

A preformulation investigation was conducted by varying the feed ratio of mAb:HA-PEG (weight ratio) from 4:1 to 1:4. mAb-MHP by adding 1 mL of HA-PEG (0.25, 0.5, 1, 2, or 4 mg/mL) dropwise to 1 mL of the mAb-MOF solution containing mAb at 1 mg/mL under vigorous stirring for 20 min. The mixture was sonicated using a Branson 450 Digital Sonifier® (10 % amplitude, 30 s, 5 s on, 5 s off) and then centrifuged at 12,000 x *g* for 15 min. The pellet was collected and resuspended in water by sonication (10 % amplitude, 30 s, 5 s on, 5 s off) to obtain the formulations. Particle size and zeta potential were measured by dynamic light scattering (DLS, Malvern Zetasizer, UK) and morphology was examined by transmission electron microscopy. mAb-MHA and mAb-MPEG were prepared using the same procedure, replacing HA-PEG with HA (1 mL, 1 mg/mL) or DSPE-PEG (1 mL, 1 mg/mL), respectively. ^{1}H NMR spectra of the formulations were recorded with a Bruker Ultrashield Advance II 400 MHz instrument in D_2O (5 mg/mL).

2.5. HA quantification

HA was quantified based on the formation of a complex between HA and cetyltrimethylammonium bromide (CTAB) as previously described [35]. The supernatant obtained after centrifugation of the formulation preparation was collected for free HA quantification. Briefly, 50 μL of the supernatant or HA calibrators (HA-PEG or HA, 15.625–1000 μg/mL) was added to each well (clear 96-well flat-bottom plate). Then, 50 μL of acetate buffer (0.2 M sodium acetate and acetic acid, 0.15 M sodium chloride, pH 6.0) was added, and the plate was incubated at 37 °C for 15 min. Then, 100 μL of 2 % (*w/v*) CTAB in 2 % (w/v) sodium hydroxide was added to each well, followed by shaking on a Rotamax platform shaker (Heidolph, Germany) for 1 min. Absorbance was measured at 600 nm using a SpectraMax® plate reader (Molecular Devices, USA). Integrated HA content within the formulation was calculated using the equation below:

$$HA\ modification\ content\ (\%) = \frac{Total\ amount\ of\ HA - free\ HA}{Total\ weight\ of\ formulation} \times 100$$

2.6. PEG quantification

PEG was quantified based on the complex formed by PEG and barium iodide as previously reported [36]. The supernatant collected after centrifugation of the formulation preparation was used for free PEG quantification. First, 100 μL of the supernatant or PEG calibrators (HA-PEG or DSPE-PEG, 1.87–120 μg/mL) was added to each well (clear 96-well flat-bottom plate). Then, 25 μL of 5 % (*w/v*) barium chloride in 1 M hydrochloric acid was added, followed by the addition of 25 μL of 1.3 % (w/v) iodine in 2 % (w/v) potassium iodide. The plate was incubated at room temperature for 15 min. Absorbance was measured at 535 nm using a SpectraMax® plate reader (Molecular Devices, USA). Integrated PEG content within the formulation was calculated using the equation below:

$$PEG\ modification\ content\ (\%) = \frac{Total\ amount\ of\ PEG - free\ PEG}{Total\ weight\ of\ formulation} \times 100$$

2.7. Storage stability of the nanosystem

The storage stability of the formulations, including mAb-MOF, mAb-MHA, mAb-MPEG, and mAb-MHP, was studied at 4 °C for 48 h. At predetermined time points, samples were withdrawn and analyzed by DLS (Malvern Zetasizer, UK).

2.8. Drug release in biomimetic GI fluids in vitro

The drug release profiles of the formulations, including mAb-MOF, mAb-MHA, mAb-MPEG, and mAb-MHP, were studied in fasted-state simulated gastric fluid (FaSSGF) for 2 h, in fasted-state simulated intestinal fluid (FaSSIF) for 6 h, and in fasted-state simulated colonic fluid (FaSSCF) for 10 h. Given the absence of standardized protocols for enzyme concentrations and activities in simulated GI fluids, particularly under IBD pathological conditions, we employed commercially available biomimetic GI fluids from Biorelevant (FaSSIF and FaSSCF) that reproduce the physicochemical characteristics of the fasted-state GI environment, including pH, bile salt, and lipid composition. Notably, biomimetic GI fluids with representative pH values (FaSSGF, pH 1.6; FaSSIF, pH 6.5; FaSSCF, pH 7.8) were used to evaluate the pH-responsive colon-targeting ability of the formulations. The compositions of the FaSSGF, FaSSIF, and FaSSCF are shown in Table S1. The formulations were dispersed in 5 mL of biomimetic GI fluid and maintained at 37 °C with gentle agitation (100 rpm). At predetermined time points (0, 0.5, 1, and 2 h for FaSSGF; 0, 1, 2, and 4 h for FaSSIF; and 0, 2, 4, 7, and 10 h for FaSSCF), 500 μL samples were collected and replaced with fresh prewarmed media. The aliquots were then centrifuged at 20,000 x *g* for 10 min. The mAb concentration in the supernatant was analyzed using a Bradford protein assay kit (Thermo Scientific, USA).

2.9. Nanosystem stability in biomimetic GI fluids in vitro

The stability of the formulations, including mAb-MOF, mAb-MHA, mAb-MPEG, and mAb-MHP, was studied in FaSSGF for 2 h, in FaSSIF for 6 h, and in FaSSCF for 10 h. The formulations were dispersed in 5 mL of biomimetic GI fluid and maintained at 37 °C with gentle agitation (100 rpm). At predetermined time points, samples were withdrawn and analyzed by DLS (Malvern Zetasizer, UK).

2.10. Lyophilization

Freshly prepared formulations were resuspended in water, 3 % sucrose, 5 % sucrose, 3 % trehalose, or 5 % trehalose. The formulations were then frozen at −20 °C for 12 h, followed by lyophilization at −38 °C and 0.238 mBar for 48 h with a freeze-dryer (Labconco, USA).

2.11. Cell culture

The J774A.1 murine macrophage cell line was cultured in RPMI-1640 medium, which was supplemented with 10 % fetal bovine serum and 1 % penicillin-streptomycin. The cells were grown in 75 cm^2 flasks and maintained at 37 °C in an incubator (BINDER GmbH, Germany) with an atmosphere of 5 % CO_2 and 95 % relative humidity. The culture medium was replaced every other day, and cells were passaged when they reached 80 % confluence.

2.12. Cell viability study

The cytotoxicity of mAb-MOF and its variants with different coatings, including mAb-MHA, mAb-MPEG, and mAb-MHP, was evaluated in J774A.1 cells using the MTT assay. In brief, 20,000 cells were seeded into each well of a 96-well plate and allowed to adhere overnight. The cells were treated with 100 μL of various concentrations of nanoparticles (ranging from 0 to 2500 μg/mL of mAb) for 6 h at 37 °C. Then the cells were washed with PBS, and a 0.5 mg/mL MTT solution was added to each well, followed by a 3-h incubation at 37 °C. The MTT solution was then removed, and 100 μL of DMSO was added to dissolve the formazan crystals. Absorbance was measured at 560 nm using a SpectraMax® plate reader (Molecular Devices, USA).

2.13. Anti-inflammatory study in vitro

The *in vitro* anti-inflammatory activity of the nanoparticles was assessed in J774A.1 cells under two conditions: (1) using mAb-MOF at varying mAb concentrations (1 to 500 μg/mL) and (2) using mAb-MOF, mAb-MHA, mAb-MPEG, and mAb-MHP at a fixed mAb concentration of 100 μg/mL. A total of 200,000 cells were seeded into each well of a 24-well plate and allowed to adhere overnight. The following day, the cells were washed with PBS and treated with 500 μL of LPS (100 ng/mL) in cell culture medium for 8 h to induce inflammation. Subsequently, 10 μL of nanoparticles was added to the cells and incubated for 4 h. The supernatants were then collected and centrifuged to remove debris. TNF-α level in the supernatants were measured using a mouse TNF-α ELISA kit (Meso Scale Discovery, USA) according to the manufacturer's instructions. IL-6, MCP-1, and MIP-1α levels were quantified using a V-PLEX Custom Mouse Biomarker ELISA Kit (Meso Scale Discovery, USA) following the manufacturer's protocol.

2.14. In vitro antioxidant study

The *in vitro* antioxidant capacity of the nanoparticles was evaluated in J774A.1 cells under two different conditions: (1) with mAb-MOF at varying Mn concentrations (0.8 to 400 μg/mL) and (2) with mAb-MOF, mAb-MHA, mAb-MPEG, and mAb-MHP at a fixed Mn concentration of 80 μg/mL. A total of 25,000 cells were seeded into each well of a black 96-well plate with a clear bottom and allowed to adhere overnight. The following day, the cells were washed with PBS and exposed to 100 μM H_2O_2 to induce oxidative stress. The nanoparticles were then added and incubated for 4 h. ROS levels were measured using 10 μM DCFH-DA (Abcam, UK) according to the manufacturer's instructions. Fluorescence intensity was measured using a SpectraMax® plate reader (Molecular Devices, USA) with excitation and emission wavelengths set at 485 nm and 535 nm, respectively.

2.15. Preparation and characterization of mAb-MHPE

ES100 was dissolved at different concentrations in 2 mL of a 2 % PVA solution supplemented with 4 mL of methanol and 0.15 mL of 1 M sodium hydroxide. Subsequently, 100 μL of mAb-MHP (100 mg/mL) was added dropwise into 1 mL of the ES100 solution (at concentrations of 0.1, 1, 5, 10, 20, and 40 mg/mL) with continuous stirring for 30 min. The nanoparticles were then collected by centrifugation at 12,000 x *g* for 15 min. The particle size and zeta potential of mAb-MHPE were characterized using DLS (Malvern Zetasizer, UK). The drug release profile and stability of mAb-MHPE in biomimetic GI fluids were studied using the aforementioned methods.

2.16. Animal studies

All animal experiments were approved by and conducted in accordance with the local animal ethics committee (2023/UCL/MD/25) and the Belgian Law of 29 May 2013 on the protection of laboratory animals. Six-week-old male C57BL/6 J mice (20–25 g) were obtained from Janvier Laboratories, France. The animals were housed under standard conditions and provided with food and sterilized tap water for a 2-week acclimation period prior to the experiments.

2.17. Evaluation of mAb-MHP efficacy in an acute murine DSS-induced colitis model

Mice were randomly divided into nine groups ($n = 8$ per group): healthy control, DSS-induced colitis group, mAb intravenous (i.v.) (mice receiving intravenous mAb and DSS), mAb oral (mice receiving oral mAb and DSS), MOF (mice receiving oral MOF and DSS), mAb-MOF (mice receiving oral mAb-MOF and DSS), mAb-MHA (mice receiving oral mAb-MHA and DSS), mAb-MPEG (mice receiving oral mAb-MPEG

and DSS), and mAb-MHP (mice receiving oral mAb-MHP and DSS). Colitis was induced by administering 3 % (*w/v*) DSS in the drinking water for five consecutive days. From Day 1 to Day 6, the mice were orally administered 100–150 μL of nanoparticle suspensions, delivering a mAb dose of 10 mg/kg. Untreated controls received water. On Day 7, the mice were anesthetized with isoflurane and evaluated *via* colonoscopy. Subsequently, the mice were euthanized, and colon tissues were collected for further analysis. The body weight of mice was measured every day from Day 1 to Day 7 and it was normalized to the initial day.

2.18. Evaluation of mAb-MHP efficacy in an acute murine TNBS-induced colitis model

Mice were randomly allocated to nine groups ($n = 8$ per group): healthy control, TNBS control, mAb intravenous (i.v.) + TNBS, mAb oral + TNBS, MOF + TNBS, mAb-MOF + TNBS, mAb-MHA + TNBS, mAb-MPEG + TNBS, and mAb-MHP + TNBS. Colitis was induced by administering 50 μL of TNBS (100 mg/kg in 0.9 % NaCl-ethanol, 50:50 *v/v*) intrarectally under isoflurane anesthesia. On Days 1 and 2, the mice received oral doses of nanoparticle formulations (100–150 μL, equivalent to 10 mg/kg mAb), while the untreated control group received water. On Day 3, colitis severity was assessed *via* colonoscopy under isoflurane anesthesia. Following this, the mice were euthanized, and colon tissues were harvested for further analysis of colitis severity.

2.19. In vivo evaluation of mAb-MHPE efficacy in an acute murine DSS-induced colitis model

Mice were randomly assigned to four groups (8 mice per group): healthy control, DSS control, oral mAb-MHP + DSS, and oral mAb-MHP + DSS. Colitis was induced by administering 3 % (*w/v*) DSS in the drinking water for five consecutive days. From Day 1 to Day 6, the mice received oral doses of 100–150 μL of the formulations (mAb dose: 10 mg/kg). On Day 7, the mice were anesthetized with isoflurane, and colitis severity was evaluated *via* colonoscopy. Blood samples were then collected from the portal vein. Finally, the mice were euthanized, and colon tissues were harvested for further analysis.

2.20. In vivo evaluation of mAb-MHPE efficacy in a chronic murine DSS-induced colitis model

Chronic colitis was induced in mice through three cycles of 3 % (*w/v*) DSS treatment, each lasting 7 days, with a 14-day washout period between cycles [37]. The mice were randomly assigned to six groups ($n = 8$ per group): healthy control, DSS control, oral mAb + DSS, oral mAb-MHP + DSS, oral MHPE + DSS, and oral mAb-MHPE + DSS. From Day 4 to Day 11 of the second and third DSS cycles, the mice were administered 100–150 μL of the formulation, corresponding to a mAb dose of 10 mg/kg. On Day 53, the mice were anesthetized with isoflurane for colonoscopy to assess colitis severity. Subsequently, the mice were euthanized, and colon tissues were collected for further evaluation of colitis severity. The body weight was measured every other day from Day 1 to Day 53 and it was normalized to the initial day.

2.21. High-resolution colonoscopy in live mice

In vivo colonoscopy was performed on mice using the Coloview® system (Karl Storz, Tuttlingen, DE). On the sacrifice day, the mice were anesthetized with isoflurane, and a mini-endoscope was carefully inserted through the anus. The colon was insufflated with air, enabling video recording and image capture for each mouse. The severity of colitis was assessed using the murine endoscopic index of colitis severity (MEICS), which evaluates five parameters: colon thickening, vascular pattern alterations, presence of fibrin, mucosal surface granularity, and stool consistency. Each parameter was scored on a scale from 0 to 3, reflecting the severity of the disease [38].

2.22. Histological scoring

Histological scoring was conducted on hematoxylin and eosin (H&E)-stained slides. The scoring system assessed various parameters: the extent of inflammatory cell infiltration, goblet cell depletion, crypt density, crypt hyperplasia, muscle layer thickening, submucosal inflammation, crypt abscess formation, and ulceration. Each parameter was graded on a scale from 0 to 3, indicating the severity of the observed histopathological change [39].

2.23. Myeloperoxidase activity

MPO activity was assessed according to the protocol established by Hanning *et al.* [40]. Colonic tissue samples were placed in 1.5 mL Eppendorf tubes containing 500 μL of HTAB buffer (0.5 % HTAB in 50 mM potassium phosphate buffer, pH 6) and homogenized on ice using a Branson 450 digital sonifier® (30 % amplitude, 10 s). The homogenates were centrifuged at 20,000 x *g* for 10 min at 4 °C. Aliquots of the supernatant (7, 14, or 21 μL) were then transferred to 96-well plates and mixed with 200 μL of MPO assay solution (50 mM potassium phosphate buffer, pH 6, containing 0.167 mg/mL *o*-dianisidine and 500 ppm H_2O_2). MPO activity was quantified by measuring absorbance at 460 nm over 30 min using a SpectraMax® plate reader (Molecular Devices, USA). MPO levels were normalized to total protein content, determined using a Pierce™ BCA Protein Assay Kit (Sigma–Aldrich, USA).

2.24. ROS intensity

Colonic ROS levels were quantified using the DCFDA method [41]. Colonic samples were put in 1 mL of Tris-HCl buffer (50 mM, pH 7.4) on ice and homogenized using a Branson 450 digital sonifier®. The homogenates were centrifuged (2,700 x *g*, 15 min, 4 °C). 50 μL of the supernatant was transferred to a black 96-well plate and incubated with 50 μL of DCFH-DA (10 μM) solution for 30 min at 37 °C. Fluorescence intensity was measured by a SpectraMax® plate reader (Molecular Devices, USA) with excitation and emission wavelengths of 485 nm and 535 nm, respectively. The results were normalized to total protein content, determined using a Pierce™ BCA Protein Assay Kit (Sigma–Aldrich, USA).

2.25. Cytokine and chemokine quantification by ELISA

Colonic tissue samples were homogenized in ice-cold lysis buffer containing 500 mM NaCl, 2 mM EDTA, 1 % Triton X-100, 0.5 % sodium deoxycholic acid, 0.1 % SDS, 50 mM Tris-HCl, and protease inhibitors. Then, the samples were sonicated using a Branson 450 digital sonifier® (Marshall Scientific, US) at 30 % amplitude for 10 s. The homogenates were then centrifuged at 20,000 x *g* for 10 min, and the supernatant was collected for the cytokine quantification. The levels of cytokines and chemokines in the colon, including IFN-γ, IL-1β, IL-6, KC/GRO, IP-10, MCP-1, MIP-1α, and TNF-α, were quantified using V-PLEX Custom Mouse Biomarker ELISA Kits (Meso Scale Discovery, USA) according to the manufacturer's instructions. All measurements were normalized to protein content, determined using a Pierce™ BCA Protein Assay Kit (Sigma–Aldrich, USA).

2.26. Real-time qPCR analysis

RNA extraction from colon tissues was performed using TRIzol reagent according to manufacturer's guidelines. The RNA was purified using lithium chloride following the method described by Viennois *et al.* [42]. cDNA synthesis was carried out using the Promega GoScript Reverse Transcription Kit (Promega Benelux BV). The program was set as follows: primers were annealed at 25 °C, DNA were polymerized at 42 °C for 1 h, and enzymes were inactivated at 70 °C for 15 min. qPCR was performed using the Promega GoTaq qPCR Master Mix on a

QIAquant 96 2plex (QIAGEN GmbH, Germany). The qPCR protocol included 45 cycles of denaturation at 95 °C for 3 s, primer annealing at 60 °C for 26 s, and extension at 72 °C for 10 s. A melting curve analysis was conducted post-amplification to ensure reaction specificity. 60S ribosomal protein L19 (RPL19) was used as the reference gene. Results were calculated relative to the control group using the delta-delta Ct method [43]. Primer sequences are provided in Table S2.

2.27. Statistical analysis

Statistical analyses were conducted using GraphPad Prism 10 (CA, USA). The Grubbs test was utilized to identify and exclude outliers within each group. For multiple group comparisons, one-way ANOVA followed by Tukey's *post hoc* test was employed. If significant variance differences were observed between groups, Kruskal–Wallis test followed by Dunn's *post hoc* test was performed. Differences between two groups were analyzed using the *t*-test. If the dependent variable was not normally distributed, the Mann–Whitney test was used instead. Results are presented as mean ± standard errors of the mean (SEM). A *p*-value of less than 0.05 was considered statistically significant.

3. Results and discussion

3.1. Preparation and characterization of an oral MOF-based antibody delivery nanosystem

An mAb-MOF was synthesized using a biomineralization-like approach, wherein the mAb interacted with Mn and 2-methylimidazole

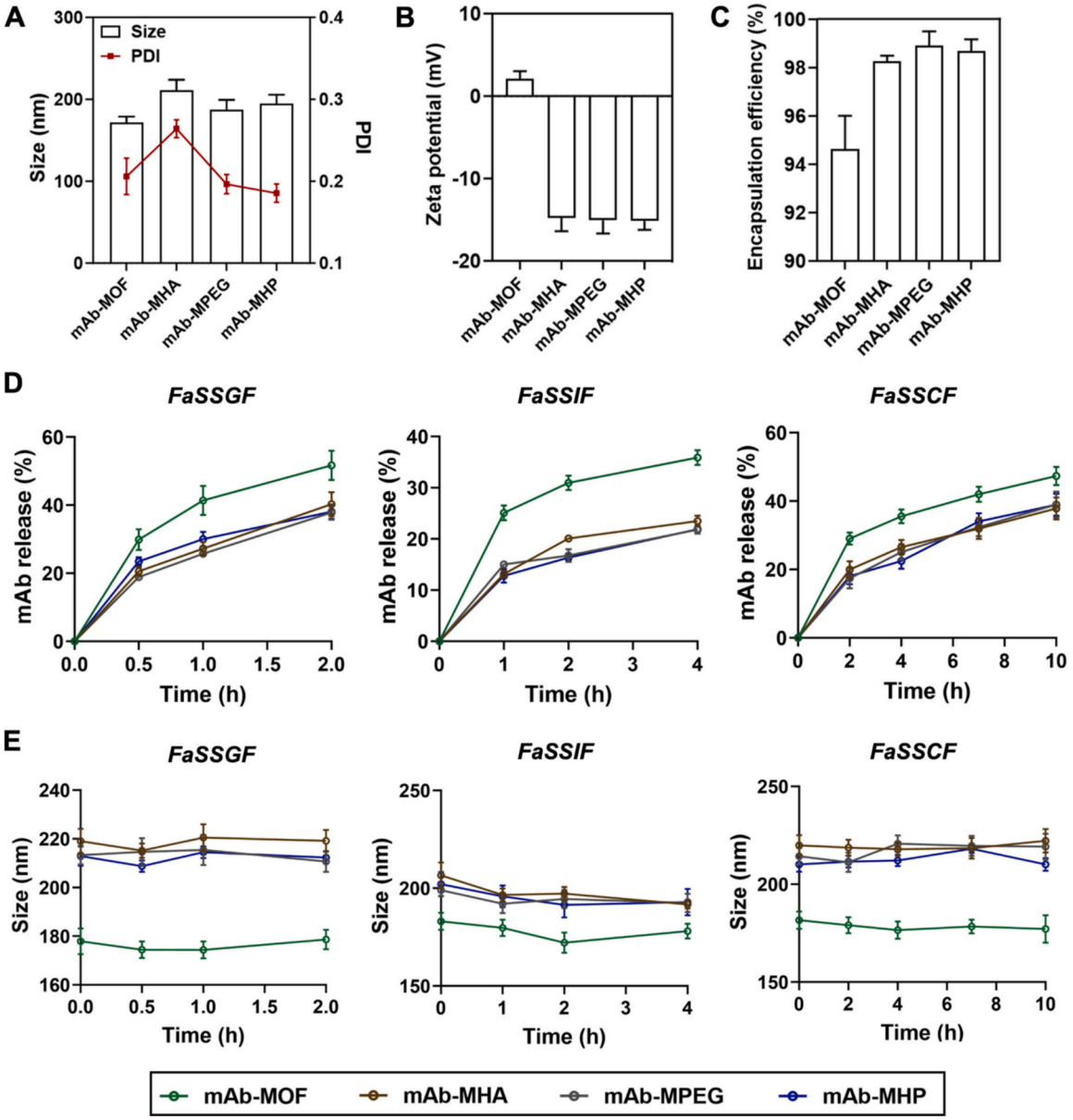

Fig. 1. Preparation and characterization of oral MOF-based antibody delivery nanosystems. (A) Particle size, polydispersity index (PDI), and (B) zeta potential of mAb-MOF and mAb-MOF with different surface coatings. mAb-MHA: mAb-MOF coated with HA. mAb-MPEG: mAb-MOF coated with PEG. mAb-MHP: mAb-MOF coated with HA-PEG (mean ± SEM; $n = 9$ from 3 independent experiments). (C) Encapsulation efficiency of mAbs in mAb-MOF, mAb-MHA, mAb-MPEG, and mAb-MHP (mean ± SEM; n = 9 from 3 independent experiments). (D) mAb release profiles of mAb-MOF, mAb-MHA, mAb-MPEG, and mAb-MHP in biomimetic gastrointestinal fluids, including fasted-state simulated gastric fluid (FaSSGF), fasted-state simulated intestinal fluid (FaSSIF), and fasted-state simulated colonic fluid (FaSSCF) (mean ± SEM; n = 9 from 3 independent experiments). (E) Variations in the particle sizes of mAb-MOF, mAb-MHA, mAb-MPEG, and mAb-MHP following an incubation in FaSSGF, FaSSIF, and FaSSCF for predetermined time intervals (mean ± SEM; n = 9 from 3 independent experiments).

(2-MIM), providing scaffolds for the formation of the MOF [44]. Previous studies have suggested that the antioxidant activity of Mn-based nanozymes increases as the valency of Mn increases to +4 [30]. To this end, H_2O_2 was introduced to oxidize the Mn in the mAb-MOF, and the X-ray photoelectron spectroscopy (XPS) analysis revealed that Mn^{4+} prevailed (Fig. S1). The mAb-MOF presented a particle size of 171.5 ± 7.3 nm (Fig. 1A) and a high mAb encapsulation efficiency of 94.64 % ± 1.38 % (Fig. 1C). Transmission electron microscopy (TEM) was used to study the morphology of the mAb-MOF, confirming its homogenous distribution (Fig. S2). Given that the therapeutic action of the mAb requires the neutralization of TNF-α, we evaluated its ability to bind to TNF-α *via* a competitive binding enzyme-linked immunosorbent assay (ELISA) [34]. The results revealed that the inhibition curve of the mAb-MOF aligned with that of the free mAb, indicating that the mAb was successfully integrated into the MOF without compromising its binding activity (Fig. S3).

Three different polymers were employed to functionalize and increase the oral efficiency of the mAb-MOF: HA for mucoadhesion *via* hydrogen bonding with mucin. Specifically, high molecular weight HA (1 MDa) was chosen for disease targeting through the HA-cluster of differentiation 44 (CD44) interaction, and for anti-inflammatory effects by preventing interaction between Toll-like receptors 2 and 4 (TLR2/4) and pathogen-associated molecular patterns (PAMPs) (the formulation was referred to as mAb-MHA) [32,45]; PEGylation for mucopenetration owing to its uncharged and hydrophilic nature (the formulation was referred to as mAb-MPEG) [31]; and an HA-PEG conjugate of both coatings (the formulation was referred to as mAb-MHP). The formulation composition of mAb-MHP was optimized by varying the feed ratio of mAb:HA-PEG from 4:1 to 1:4. The ratio of 1:1 was selected, as further increases in HA-PEG concentration did not significantly change the particle size or zeta potential (Fig. S4). The same ratio was applied for the preparation of mAb-MHA and mAb-MPEG. The characterization of the formulations by dynamic light scattering (DLS) revealed that the polymer-coated mAb-MOF, including mAb-MHA (size: 211.2 ± 12.7 nm, zeta potential: −14.78 ± 1.61 mV), mAb-MPEG (184.0 ± 12.9 nm, −15.06 ± 1.62 mV), and mAb-MHP (194.12 ± 11.4 nm, − 15.15 ± 1.07 mV), exhibited larger hydrodynamic sizes and more negative surface charges than the uncoated mAb-MOF (171.5 ± 7.3 nm, 2.06 ± 0.97 mV), indicating successful polymer coating (Fig. 1A and B). In addition, the quantification of HA and PEG showed that mAb-MHP contained 10.71 ± 1.32 % of HA and 2.48 ± 0.38 % of PEG, mAb-MHA contained 13.23 ± 2.15 % of HA, and mAb-MPEG contained 11.08 ± 1.69 % of PEG (Fig. S5). ^{1}H NMR further confirmed the presence of HA and/or PEG in the coated formulations (Fig. S6-S8). In addition, the polymer coatings improved the storage stability of the formulations, with PEGylation further increasing the stability (Fig. S9).

The profile of mAb release from the formulations was evaluated in biomimetic GI fluids. Three conditions were employed to mimic the transit of the formulations in the GIT: incubation in fasted-state simulated gastric fluid (FaSSGF) for 2 h, incubation in fasted-state simulated intestinal fluid (FaSSIF) for 4 h, and incubation in fasted-state simulated colonic fluid (FaSSCF) for 10 h. Compared with the mAb-MOF, the rates of mAb and Mn release from the mAb-MHA, mAb-MPEG, and mAb-MHP were lower in these biomimetic GI fluids (Fig. 1D and Fig. S10), probably due to the steric hindrance of the polymer coating on the MOF surface. In addition, all formulations loaded with mAbs were stable *in vitro* in the different simulated GI fluids (Fig. 1E).

3.2. *In vitro anti-inflammatory and antioxidant effects of the MOF on J774A.1 macrophages*

The cytotoxicity of the formulations was evaluated in the J774A.1 murine macrophage line. mAb-MOF and mAb-MHP demonstrated good biocompatibility, with cell viability exceeding 80 % within the mAb concentration range of 0–2500 μg/mL (Fig. S11). The anti-inflammatory and antioxidant effects of different doses of mAb-MOF were evaluated in J774A.1 cells. Since the antibody neutralizes TNF-α, we interpret the reduction as a result of functional inhibition rather than decreased expression. Treatment with mAb-MOF significantly decreased TNF-α levels in lipopolysaccharide (LPS)-stimulated cells within the mAb concentration range of 1–500 μg/mL (Fig. 2B). Moreover, mAb-MOF treatment significantly decreased the intracellular ROS levels in hydrogen peroxide (H_2O_2)-stimulated cells when the Mn concentration ranged from 0.8 to 400 μg/mL (Fig. 2D). A concentration-dependent antioxidant effect was observed, with superior ROS scavenging achieved at Mn concentrations of 80–400 μg/mL (Fig. 2D). The anti-inflammatory and antioxidant effects of the different formulations were further compared at concentrations of 100 μg/mL mAb and 80 μg/mL Mn. All the formulations, including mAb-MOF, mAb-MHA, mAb-MPEG, and mAb-MHP, exhibited similar efficacy at decreasing TNF-α level in LPS-stimulated J774A.1 cells (Fig. 2C) and comparable ROS scavenging capabilities in H_2O_2-stimulated J774A.1 cells (Fig. 2E), with the mAb-MHP group showing profound TNF-α reduction (up to 57 %) and ROS scavenging (up to 44 %). Notably, mAb-MOF, mAb-MHA, mAb-MPEG, and mAb-MHP significantly suppressed the secretion of interleukin-6 (IL-6), monocyte chemoattractant protein-1 (MCP-1), and macrophage inflammatory protein-1 alpha (MIP-1α), which are key proinflammatory cytokines and chemokines involved in IBD progression, in LPS-stimulated J774A.1 cells (Fig. 2F) [46]. These results confirmed our hypothesis that mAb-MOF can alleviate IBD by acting through different pathological pathways involved in IBD.

3.3. *In vivo efficacy evaluation of the MOF in an acute DSS-induced colitis model*

Encouraged by the promising *in vitro* efficacy, we further evaluated the *in vivo* therapeutic efficacy of the formulations in a dextran sulfate sodium (DSS)-induced murine colitis model [37]. DSS (~40 kDa) disrupts tight junctions and increases intestinal permeability, facilitating the translocation of bacteria and associated antigens into the gut mucosa and triggering hyperactive immune responses [37]. The mice were provided with 3 % DSS in their drinking water for five consecutive days to induce colitis. As illustrated in Fig. 3A, all the treatments were administered orally from Day 1 to Day 6, except for the mAb intravenous (i.v.) group, which received the mAb *via* intravenous injection to mimic the clinical administration of the anti-TNF-α antibody (infliximab) [47]. mAb-MOFs with different coatings (mAb-MHA, mAb-MPEG, and mAb-MHP) were included to screen the most promising therapeutic candidates. The mice were sacrificed on Day 7, and the colons were harvested for subsequent analysis. The body weight of mice was measured daily and calculated based on the body weight on Day 1. The results revealed that the DSS-treated mice tended to experience weight loss (Fig. S12A and S12B), and the DSS group and mAb oral group presented an increased colon weight/length ratio (Fig. S12C). The macroscopic severity of colitis was assessed through a histological analysis of hematoxylin and eosin (H&E)-stained colon tissues (Fig. S13A) and high-resolution colonoscopy in live mice at the endpoint of the experiment (Fig. S13B). The DSS group presented a significant increase in both the histological score and murine endoscopic index of colitis severity (MEICS), confirming the successful establishment of the colitis model. We observed no significant differences between all the treatment groups and the DSS group, but the histological scores and MEICS scores of the mAb-MHA, mAb-MPEG, and mAb-MHP groups were reduced to similar levels as those in the mAb i.v. group (Fig. S13).

We further analyzed the colonic ROS level, evaluating the antioxidant capacity *in vivo*, and the activity of colonic myeloperoxidase (MPO), a biomarker of neutrophil infiltration (Fig. 3B and C) [40]. The ROS level and MPO activity in the mAb i.v. group were not significantly different from those in the DSS group. In contrast, treatment with mAb-MHP resulted in profound reductions in both the ROS levels (−71 %) and MPO activity (−67 %) in the mice with colitis, surpassing the reductions observed in the mAb i.v. group and the other mAb-loaded MOF

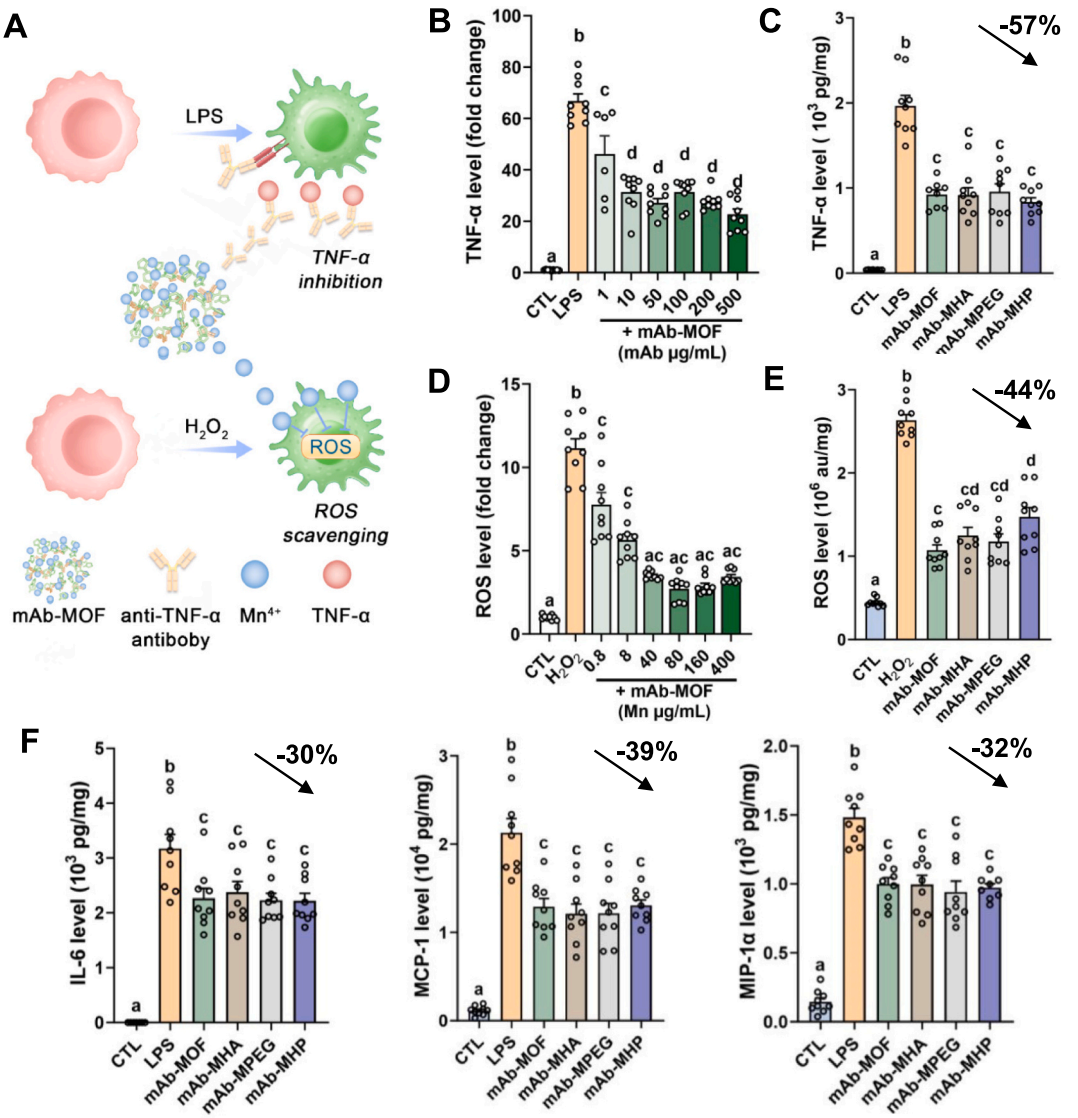

Fig. 2. *In vitro* evaluation of the anti-inflammatory and antioxidant effect of the MOF on J774A.1 macrophages. (A) Schematic illustration of the ability of the mAb-MOF to decrease TNF-α levels and scavenge ROS in activated macrophages. (B) Effect of mAb-MOF on TNF-α secretion from lipopolysaccharide (LPS)-stimulated J774A.1 cells after 4 h of treatment with increasing mAb concentrations ranging from 1 to 500 μg/mL (mean ± SEM; $n = 9$ from 3 independent experiments). (C) Effects of different formulations on TNF-α secretion in LPS-stimulated J774A.1 cells (mAb concentration: 100 μg/mL) (mean ± SEM; n = 9 from 3 independent experiments). (D) Effect of mAb-MOF on the ROS level in H_2O_2-stimulated J774A.1 cells after 4 h of treatment with increasing Mn concentrations ranging from 0.8 to 400 μg/mL. The Mn concentration in the ROS evaluation corresponded to the mAb concentration in the TNF-α evaluation (mean ± SEM; n = 9 from 3 independent experiments). (E) Effects of different formulations on the ROS levels in H_2O_2-stimulated J774A.1 cells (Mn concentration: 80 μg/mL) (mean ± SEM; n = 9 from 3 independent experiments). (F) Effects of different formulations on IL-6, MCP-1, and MIP-1α secretion by LPS-stimulated J774A.1 cells (mAb concentration: 100 μg/mL) (mean ± SEM; n = 9 from 3 independent experiments). Data with different superscript letters are significantly different (*$p < 0.05$) according to one-way analysis of variance followed by Tukey's *post hoc* test. The black arrows represent the reduction in the mAb-MHP group with respect to the LPS group.

p.o. groups (Fig. 3B and C). The colonic levels of proinflammatory cytokines, including TNF-α, IL-1β, IL-6, and interferon-gamma (IFN-γ), and chemokines, including keratinocyte chemoattractant/human growth-regulated oncogene (KC/GRO), IFN-γ-inducible protein 10 (IP-10), and MCP-1, which are known to be elevated in the DSS model [48], were quantified by ELISA (Fig. 3D and E). The DSS group presented significantly elevated levels of these cytokines and chemokines, indicating severe immune cell infiltration and immune activation in the mice with colitis. Compared with the DSS group, treatment with mAb-MOF or mAb-MOF with different coatings resulted in reduced levels of proinflammatory cytokines and chemokines. Notably, the results revealed that the levels of almost all proinflammatory cytokines and chemokines, including TNF-α, IL-1β, IL-6, IFN-γ, KC/GRO, IP-10, and MCP-1, were significantly reduced in the groups treated with the mAb-MOF with different coatings, reaching the same statistical level as the mAb i.v. group. Interestingly, in these oral treatment groups (mAb-MHA, mAb-MPEG, and mAb-MHP), the levels of proinflammatory cytokines and chemokines, such as TNF-α, IL-6, IP-10, and MCP-1, were not significantly different even from those in healthy mice. In contrast, oral mAb treatment failed to decrease the levels of the tested proinflammatory cytokines and chemokines (Fig. 3D and E). Strikingly, among all the orally administered mAb-MOF treatments, the mAb-MHP treatment (surface modified with both PEG and HA) presented the greatest anti-inflammatory effect, with significantly decreased levels of IL-1β (−65 %), KC/GRO (−41 %), and MCP-1 (−50 %), suggesting the alleviation of the proinflammatory cascade. In addition, mAb-MHA treatment significantly increased the expression of mucin 2 (MUC2), the primary gel-forming mucin in the colon, by 2.3-fold and that of the tight junction

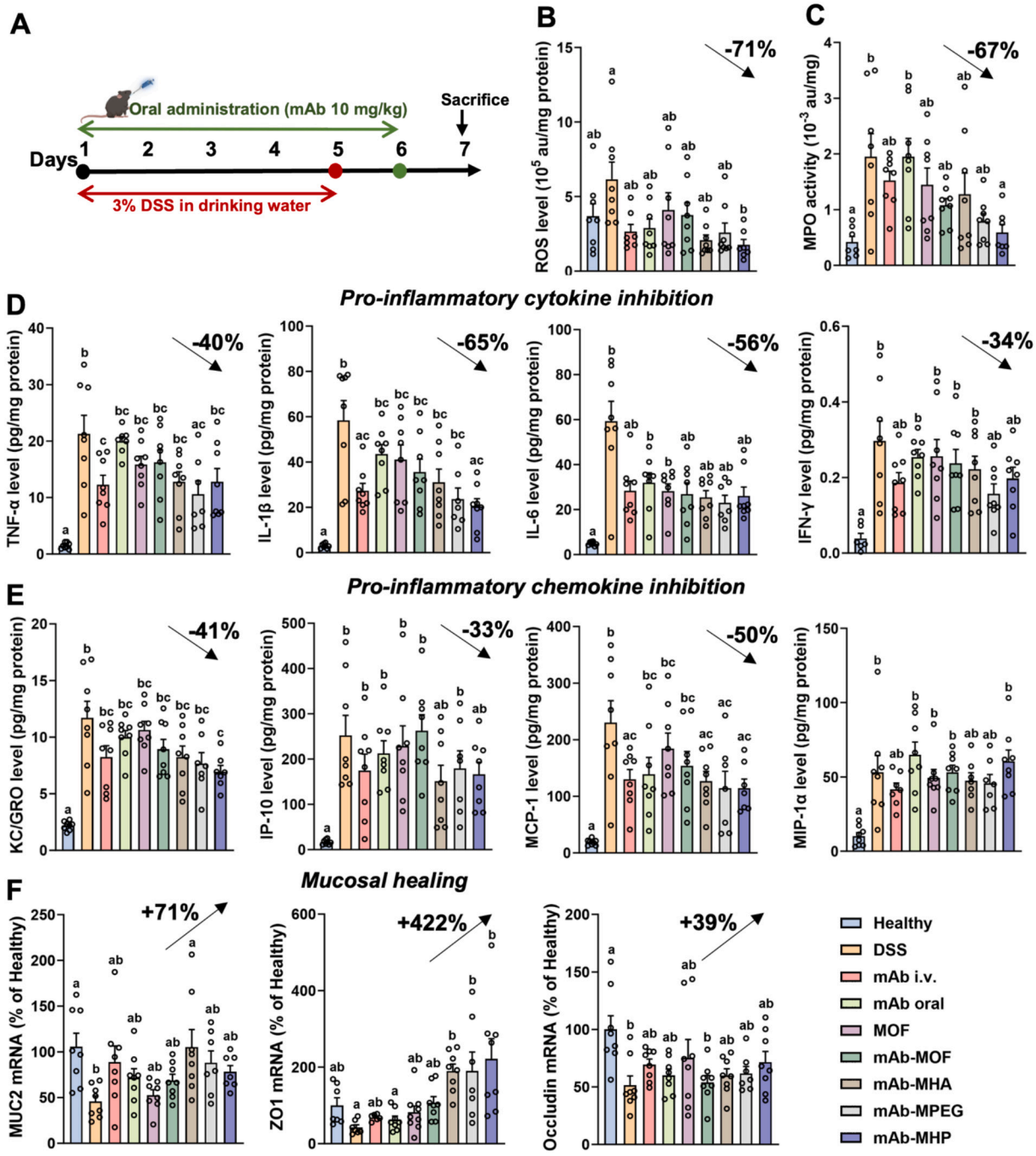

Fig. 3. *In vivo* efficacy of the oral MOF in a DSS-induced acute colitis model. (A) Schematic illustration of the DSS-induced colitis model. The mice were intravenously administered the free mAb or orally administered free mAb, MOF, mAb-MOF, mAb-MHA, mAb-MPEG, or mAb-MHP (10 mg/kg mAb) for 6 days. (B) Colonic ROS levels (mean ± SEM; $n = 7–8$). (C) Colonic myeloperoxidase (MPO) activity (mean ± SEM; n = 7–8). (D) Colonic levels of proinflammatory cytokines (TNF-α, IL-1β, IL-6, and IFN-γ) and (E) chemokines (KC/GRO, IP-10, MCP-1, and MIP-1α) were evaluated by ELISA (mean ± SEM; n = 7–8). (F) mRNA expression of gut permeability biomarkers (MUC2, ZO1, and Occludin) in the colon (mean ± SEM; n = 7–8). Data with different superscript letters are significantly different (*$p < 0.05$) according to one-way analysis of variance followed by Tukey's *post hoc* test (MPO, TNF-α, IL-1β, IFN-γ, KC/GRO, IP-10, MCP-1, MIP-1α, MUC2, and Occludin) or the Kruskal–Wallis test followed by Dunn's *post hoc* test (ZO1 and ROS). The black arrows represent a reduction or increase in the oral mAb-MHP group compared with the DSS group.

protein Zonula Occludens-1 (ZO1) by 4.5-fold, suggesting a marked attenuation of DSS-induced gut barrier disruption (Fig. 3F).

3.4. *In vivo efficacy evaluation of the MOF in an acute TNBS-induced colitis model*

We further evaluated the therapeutic efficacy of the orally administered anti-TNF-α monoclonal antibody-loaded MOFs in the TNBS-induced colitis model. This colitis model was induced by the intrarectal administration of 2,4,6-trinitrobenzene sulfonic acid (TNBS), which elicits a T-cell-mediated response against hapten-modified autologous proteins [37]. Treatments were administered orally for two days at the same dosage used in the DSS model. The mice were sacrificed on Day 3, and the colons were collected for analysis (Fig. 4A). Compared

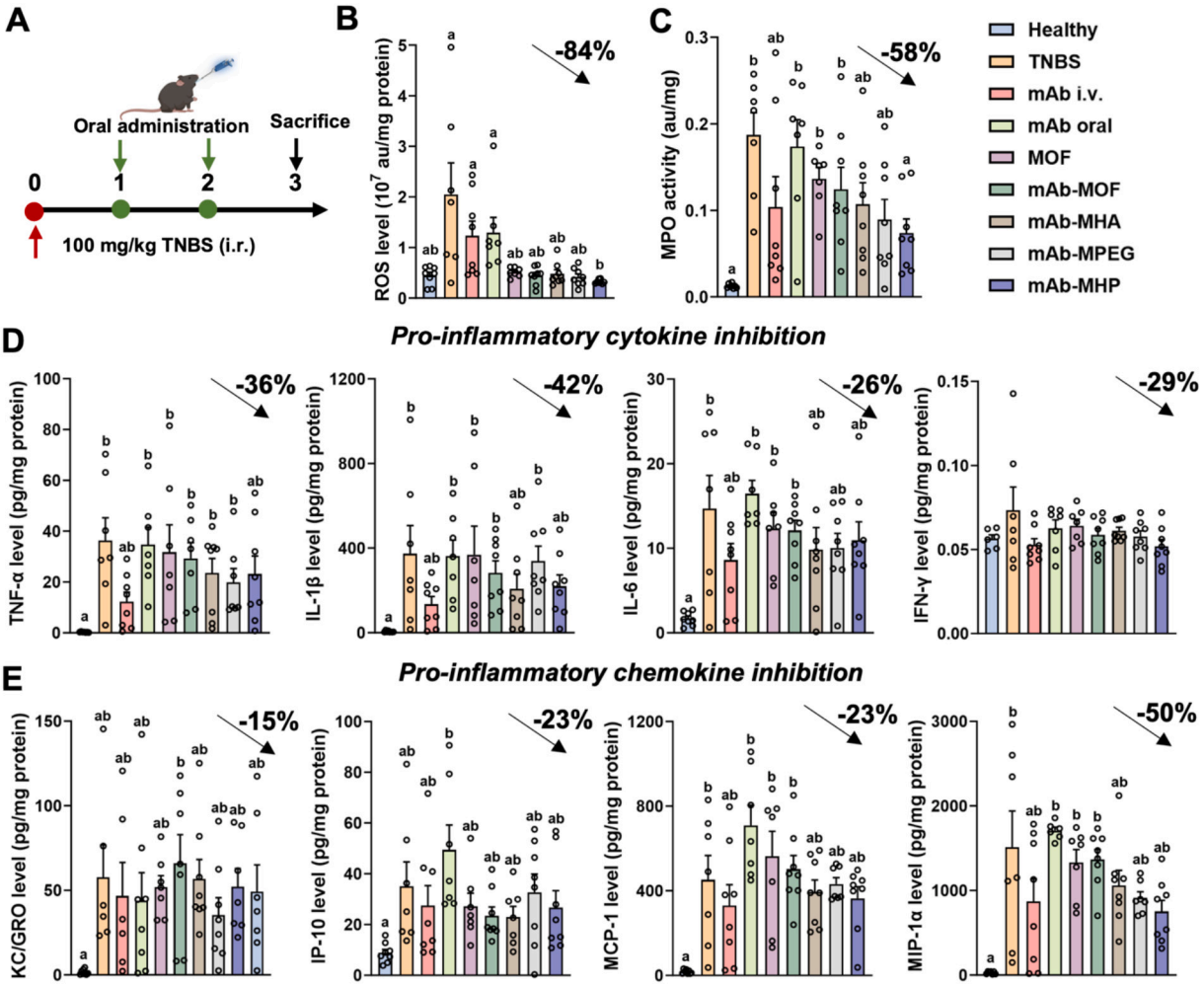

Fig. 4. *In vivo* efficacy of the oral MOF in a TNBS-induced colitis model. (A) Schematic illustration of the TNBS-induced colitis model. The mice were intravenously administered the free mAb or orally administered the free mAb, MOF, mAb-MOF, mAb-MHA, mAb-MPEG, or mAb-MHP (10 mg/kg mAb) for 2 days. (B) Colonic ROS levels (mean ± SEM; $n = 7–8$). (C) Colonic MPO activity (mean ± SEM; n = 7–8). (D) Colonic levels of proinflammatory cytokines (TNF-α, IL-1β, IL-6, and IFN-γ) and (E) chemokines (KC/GRO, IP-10, MCP-1, and MIP-1α) were evaluated by ELISA (mean ± SEM; n = 7–8). Data with different superscript letters are significantly different (*$p < 0.05$) according to one-way analysis of variance followed by Tukey's *post hoc* test (ROS, MPO, and MIP-1α) or the Kruskal–Wallis test followed by Dunn's *post hoc* test (TNF-α, IL-1β, IL-6, IFN-γ, KC/GRO, IP-10, and MCP-1). The black arrows represent the reduction in the oral mAb-MHP group compared with the DSS group.

with the TNBS group, the mAb-MOF-treated groups (mAb-MHA, mAb-MPEG, and mAb-MHP) presented no significant differences in weight loss (Fig. S14A and S14B), the colon weight/length ratio (Fig. S14C), the expression of gut permeability biomarkers (Fig. S14D), or the histological and colitis endoscopic score (MEICS) (Fig. S15A and S15B). Notably, compared with the DSS treatment, the regimen of administration was reduced, which could at least partially explain why we did not observe changes in these parameters. However, with respect to oxidative stress and inflammatory markers, the i.v. mAb treatment had no significant effect on the colonic ROS level or MPO activity, whereas the oral administration of different mAb-MOFs effectively alleviated the ROS levels and MPO activity in the colon, among which mAb-MHP had the most pronounced effect, significantly reducing the colonic ROS level (−84 %) and MPO activity (−58 %) (Fig. 4B and C). These results indicated that mAb-MHP effectively attenuated oxidative stress and alleviated neutrophil infiltration and activation at the inflamed colon site. Compared with the TNBS group, the oral mAb-MHP group presented a trend toward reduced levels of proinflammatory cytokines, including TNF-α (−36 %), IL-1β (−42 %), and IL-6 (−26 %), and chemokines, including KC/GRO (−15 %), IP-10 (−23 %), MCP-1 (−23 %), and MIP-1α (−50 %) (Fig. 4D and E).

3.5. Preparation and characterization of colon-targeting MOF-based antibody nanosystems

The mAb-MHP group exhibited promising anti-inflammatory efficacy *in vitro* and in two *in vivo* colitis models. However, considering that the rapid release of the mAb-MHP in FaSSGF (Fig. 1D) may hinder the delivery of the mAb to the inflamed colon, we introduced the colon-targeting, pH-sensitive polymer ES100 to enable the targeted delivery of the mAb to the colon. ES100 can protect the formulation from gastric acid while rapidly dissolving above pH 7.0, which mimics colonic fluid conditions, thereby enabling colon-specific release [16]. The ES100-coated mAb-MHP, named mAb-MHPE, was developed by nanoprecipitation. The composition of the mAb-MHPE formulation was optimized by adjusting the ratio of mAb-MHP to ES100, which ranged from 1:0.01 to 1:4 (*w*/w), based on the hydrodynamic size, size distribution, surface charge, and drug release profile in FaSSGF (Fig. S16). A ratio of 1:2 was selected because of the significantly decreased drug release in FaSSGF (Fig. S16D and S16F). Compared with mAb-MHP, mAb-MHPE had a larger hydrodynamic size of 243.4 ± 13.8 nm, a narrow size distribution (PDI: 0.13 ± 0.08), and a more negative zeta potential of −22.79 ± 2.18 mV (Fig. 5A and B). The morphology of

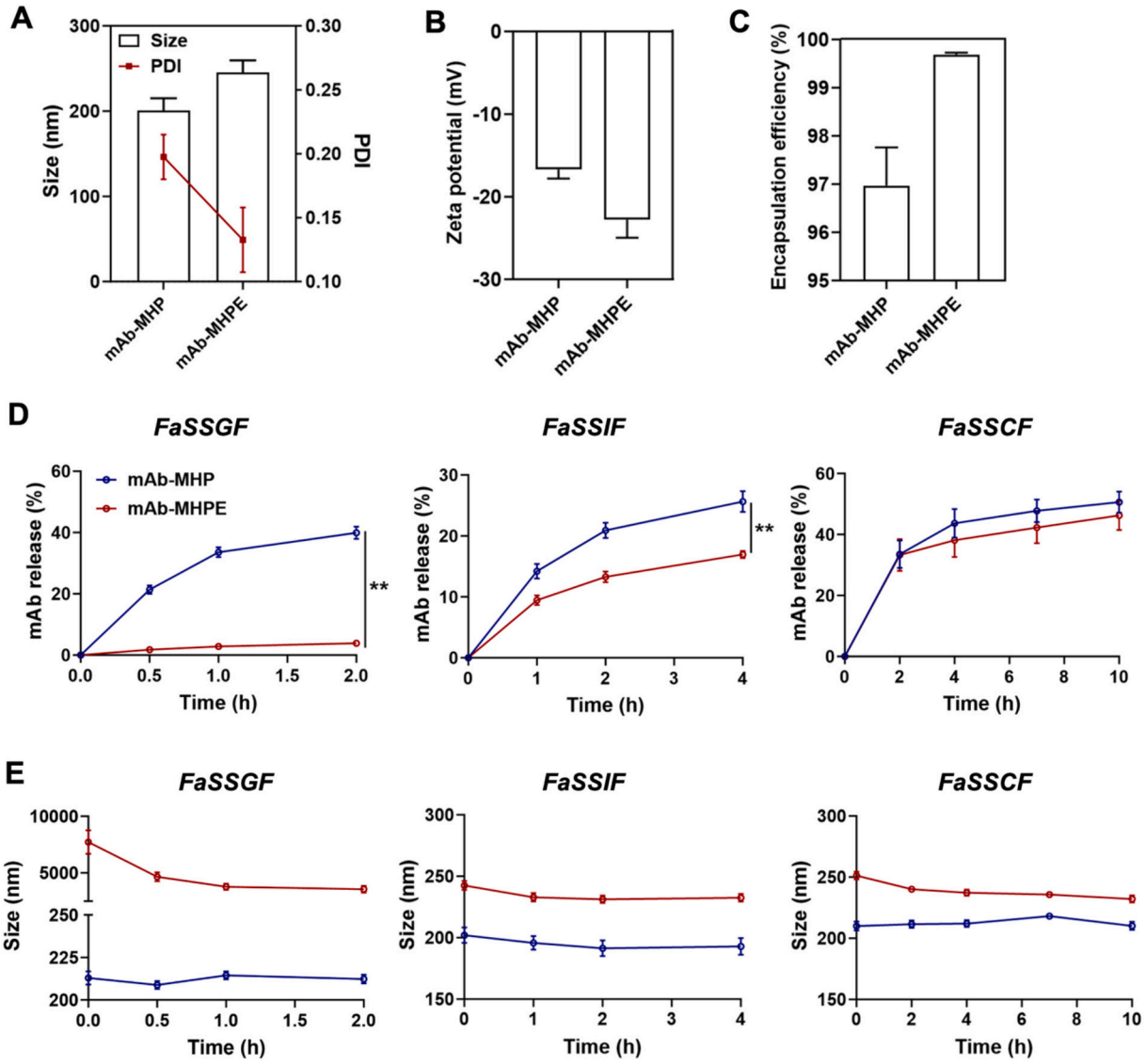

Fig. 5. Preparation and characterization of colon-targeting MOF-based antibody delivery nanosystems. (A) Particle size, polydispersity index (PDI), and (B) zeta potential of mAb-MHP and the colon-targeting mAb-MHPE (mean ± SEM; $n = 9$ from 3 independent experiments). (C) Encapsulation efficiency of mAbs in mAb-MHP and mAb-MHPE (mean ± SEM; n = 9 from 3 independent experiments). (D) mAb release profile of mAb-MHP and mAb-MHPE in biomimetic gastrointestinal fluids, including FaSSGF, FaSSIF, and FaSSCF (mean ± SEM; n = 9 from 3 independent experiments). (E) Variations in the particle sizes of mAb-MHP and mAb-MHPE following an incubation in FaSSGF, FaSSIF, and FaSSCF for predetermined time intervals (mean ± SEM; n = 9 from 3 independent experiments).

mAb-MHPE was evaluated by TEM and revealed a homogeneous distribution (Fig. S13A). Strikingly, compared with that of mAb-MHP, the mAb release from mAb-MHPE after a 2-h incubation in FaSSGF decreased significantly from 39.95 ± 6.07 % to 3.87 ± 2.29 % (Fig. 5D), indicating that the ES100 coating could successfully prevent mAb leakage during stomach transit. Moreover, compared with mAb-MHP, mAb-MHPE resulted in slower mAb and Mn release in FaSSIF while maintaining a rapid release profile in FaSSCF (Fig. 5D and Fig. S17). In addition, as shown in Fig. 5E, mAb-MHPE exhibited aggregation in FaSSGF, displaying a heterogeneous distribution (PDI: 0.47 ± 0.11) and a particle size of 3560.44 ± 908.96 nm after 2 h of incubation, likely due to the nonionizable nature of ES100 at the acidic pH of FaSSGF (pH 1.2). However, upon transfer from FaSSGF to FaSSIF (FaSSIF 0 h), mAb-MHPE disaggregated, achieving a uniform size distribution (PDI: 0.08 ± 0.02) with a particle size of 242.62 ± 11.02 nm. Furthermore, after transfer from FaSSIF to FaSSCF (FaSSCF 0 h), mAb-MHPE maintained a uniform distribution (PDI: 0.10 ± 0.04) with a size of 251.26 ± 9.66 nm. Notably, the particle size of mAb-MHPE decreased during a 10-h incubation in FaSSCF, indicating the progressive dissolution of the ES100 coating (Fig. 5E). These results confirmed the successful development of a colon-targeted nanosystem. We further optimized the lyophilization method for mAb-MHPE to facilitate clinical translation and commercialization. Various concentrations (3 % and 5 %) of cryoprotectants, including sucrose and trehalose, were evaluated. Although the size and uniform distribution of the lyophilized mAb-MHPE without cryoprotectants were maintained (Fig. S18B), the binding activity of the loaded mAb toward TNF-α was compromised (Fig. S18C). The inclusion of cryoprotectants not only maintained the size and uniform distribution of mAb-MHPE (Fig. S18B) but also preserved the binding activity of the encapsulated mAb (Fig. S18C), with 3 % sucrose selected for further use because of its cost-effectiveness compared with trehalose.

3.6. *In vivo efficacy of the colon-targeting MOF in an acute DSS-induced colitis model*

Encouraged by the promising *in vitro* release profile, we further

evaluated the therapeutic efficacy of the colon-targeted nanosystem mAb-MHPE in a murine DSS-induced acute colitis model. The construction of the model and treatment scheme were the same as those described in Section 3.3 (Fig. 3A). The mice were randomly divided into four groups: healthy (healthy mice), DSS, mAb-MHP (mice receiving oral mAb-MHP + DSS), and mAb-MHPE (mice receiving oral mAb-MHPE + DSS).

The results showed that the oral administration of mAb-MHPE alleviated weight loss (Fig. S19A and S19B) and decreased the colon weight/length ratio (Fig. S19C) in mice after 7 days of treatment, although these effects were not significantly different from those in the DSS group. Strikingly, compared with the DSS group, mAb-MHPE

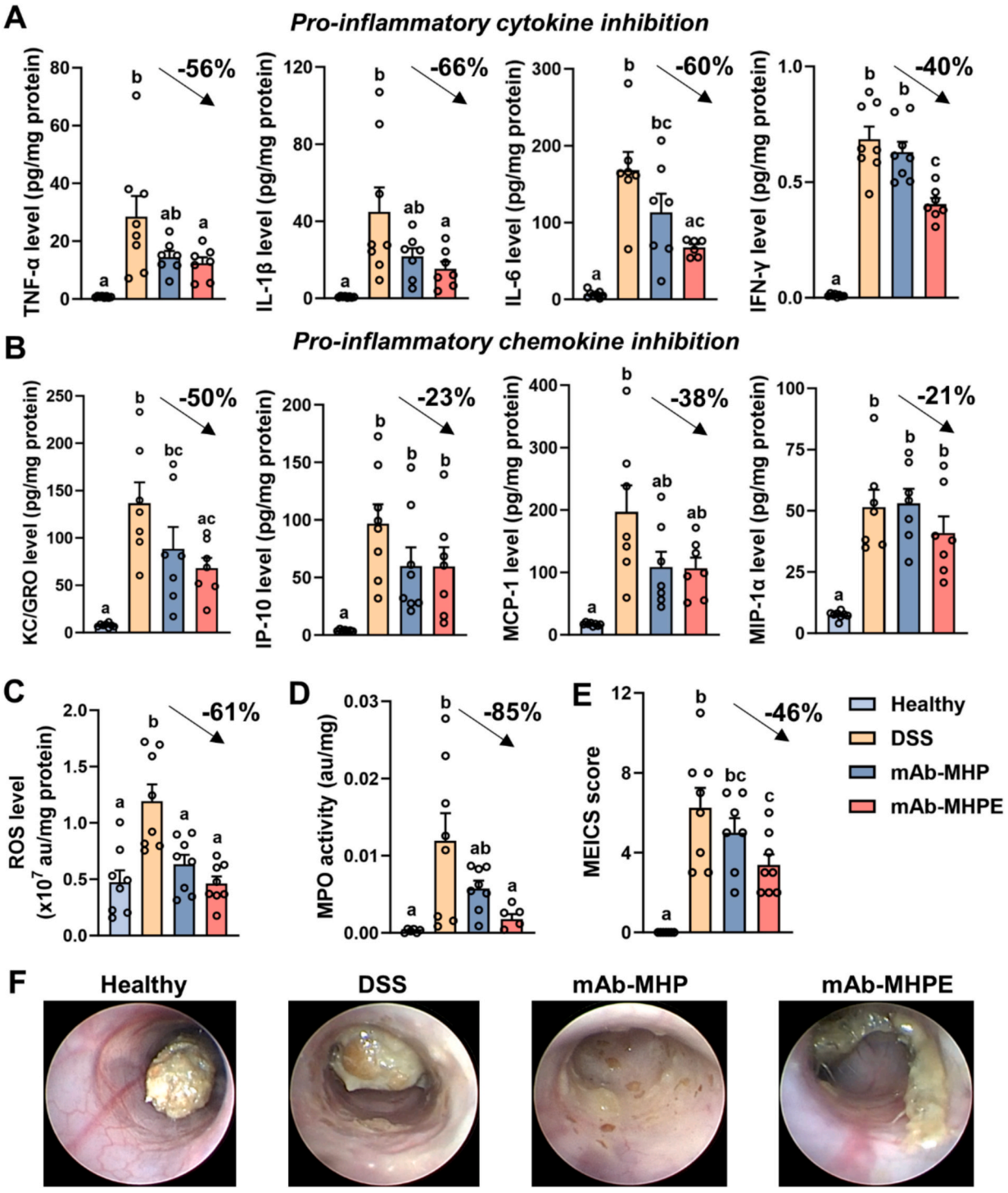

Fig. 6. *In vivo* efficacy of the colon-targeting MOF in a murine DSS-induced acute colitis model. (A) Colonic levels of proinflammatory cytokines (TNF-α, IL-1β, IL-6, and IFN-γ) and (B) chemokines (KC/GRO, IP-10, MCP-1, and MIP-1α) were evaluated by ELISA (mean ± SEM; $n = 7$–8). (C) Colonic ROS levels (mean ± SEM; $n = 8$). (D) Colonic MPO activity (mean ± SEM; $n = 6$–8). (E) Endoscopic score (murine endoscopic index of colitis severity, MEICS) of the mice on Day 7 post-treatment (mean ± SEM; n = 7–8). (F) Representative colonoscopy images (mean ± SEM; n = 6–8). Data with different superscript letters are significantly different ($^*p < 0.05$) according to one-way analysis of variance followed by Tukey's *post hoc* test. The black arrows represent the reduction in the mAb-MHPE group compared with the DSS group.

significantly decreased the colonic levels of proinflammatory cytokines (Fig. 6A), including TNF-α (−56 %), IL-1β (−66 %), IL-6 (−60 %), and IFN-γ (−40 %), as well as the proinflammatory chemokine KC/GRO (−50 %) (Fig. 6B), indicating its robust immunomodulatory effects. Remarkably, mAb-MHPE significantly reduced the colonic ROS level (−85 % compared with the DSS group, Fig. 6C) and MPO activity (−61 %, Fig. 6D) to the same levels observed in healthy mice. Compared with the DSS group, the mAb-MHPE group presented no significant differences in the mRNA expression of gut permeability biomarkers or in the histological scores (Fig. S19D and S19E). Colonoscopy is the gold standard for the assessment of disease activity in the clinic [49]. Notably, mAb-MHPE treatment resulted in a substantial reduction in the MEICS score, resulting in a decrease of up to 46 % compared with that of the DSS group, underscoring its superior anti-inflammatory efficacy (Fig. 6E). This improvement was confirmed across multiple parameters, including reduced colonic thickening, normalization of vascular patterns, alleviation of fibrin deposition, decreased granularity of the mucosal surface, and improved stool consistency (Fig. 6F).

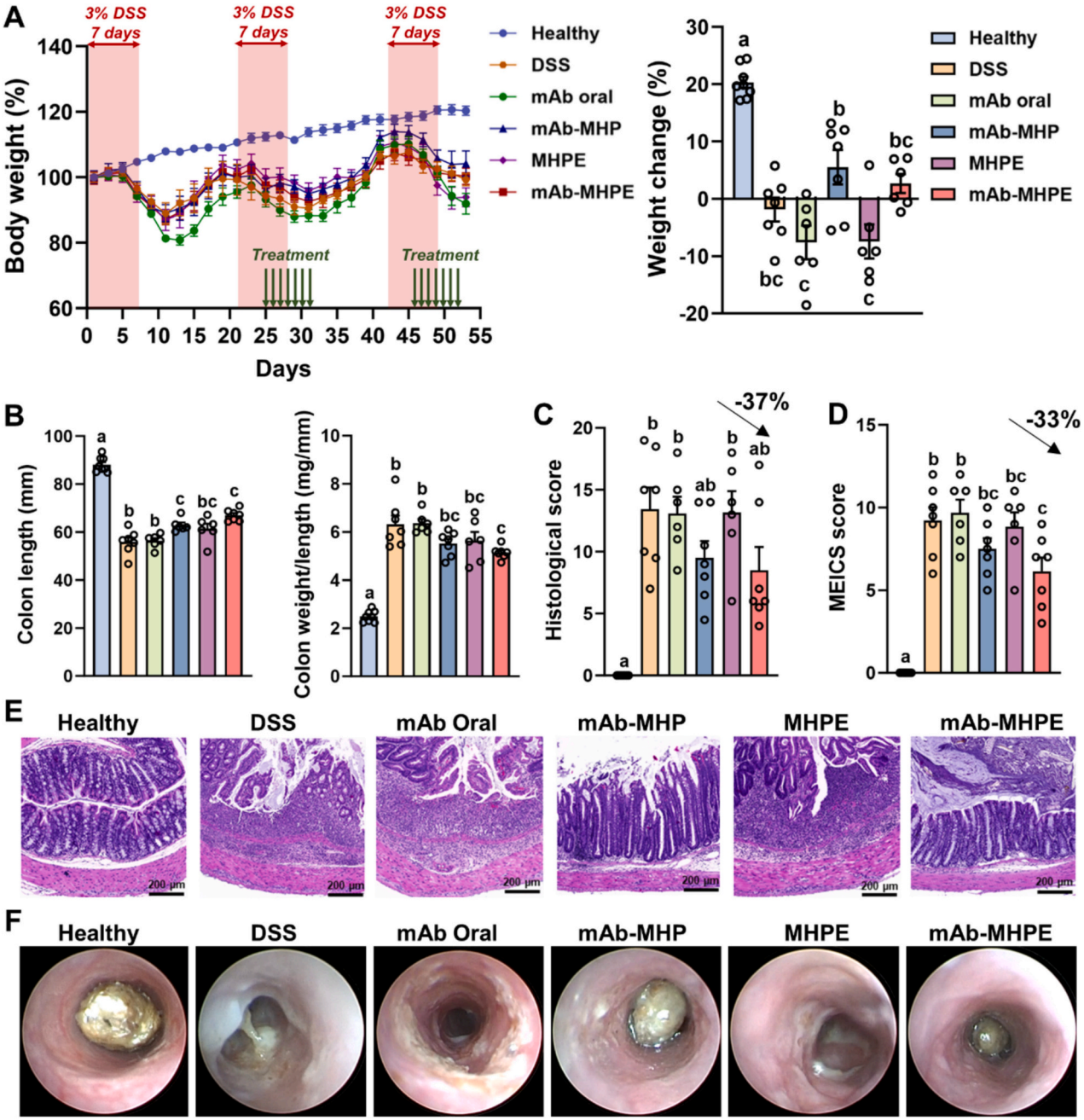

Fig. 7. *In vivo* efficacy of the colon-targeting MOF in a DSS-induced chronic colitis model. (A) Chronic colitis was induced by three cycles of 3 % DSS (7 d of DSS induction, 14 d of water). The mice were orally administered the free mAb, mAb-MHP, MHPE or mAb-MHPE from Day 4 to Day 11 of the second and third cycles. Body weight (%) over the study period (53 days). The body weight (%) over the study period (53 days) and the weight change on Day 53 compared with Day 0 are shown (mean ± SEM; n = 6–10). (B) Colon length and the colon weight/length ratio (mean ± SEM; n = 6–8). (C) Histological score indicating colitis severity (mean ± SEM; n = 6–8). (D) MEICS score on Day 53 post-treatment (mean ± SEM; n = 6–8). (E) Representative histological images of the colon (mean ± SEM; n = 6–8). (F) Representative colonoscopy images (mean ± SEM; n = 6–8). Data with different superscript letters are significantly different (*$p < 0.05$) according to one-way analysis of variance followed by Tukey's *post hoc* test. The black arrows represent the reduction in the oral mAb-MHPE group compared with the DSS group.

3.7. In vivo efficacy of the colon-targeting MOF in a chronic DSS-induced colitis model

IBD is a chronic relapsing–remitting disease characterized by alternating periods of flare-ups and remission [2]. We developed a murine model of DSS-induced chronic colitis to better recapitulate IBD progression [37]. As outlined in Fig. 7A, the model involved administering 3 % DSS in the drinking water for 7 days to induce flare-ups, followed by a 14-day washout period without DSS to simulate remission, constituting one cycle. This cycle was repeated three times to mimic the relapsing phases of the disease, with the mice being sacrificed on Day 11 of the third cycle (Day 53 of the entire model). Different treatment groups were studied, including the mAb oral, mAb-MHP, MHPE (MHPE loaded with bovine serum albumin instead of mAb), and mAb-MHPE groups, to investigate the therapeutic potential of the formulations. All the treatments were administered orally from Day 4 to Day 11 of the second and

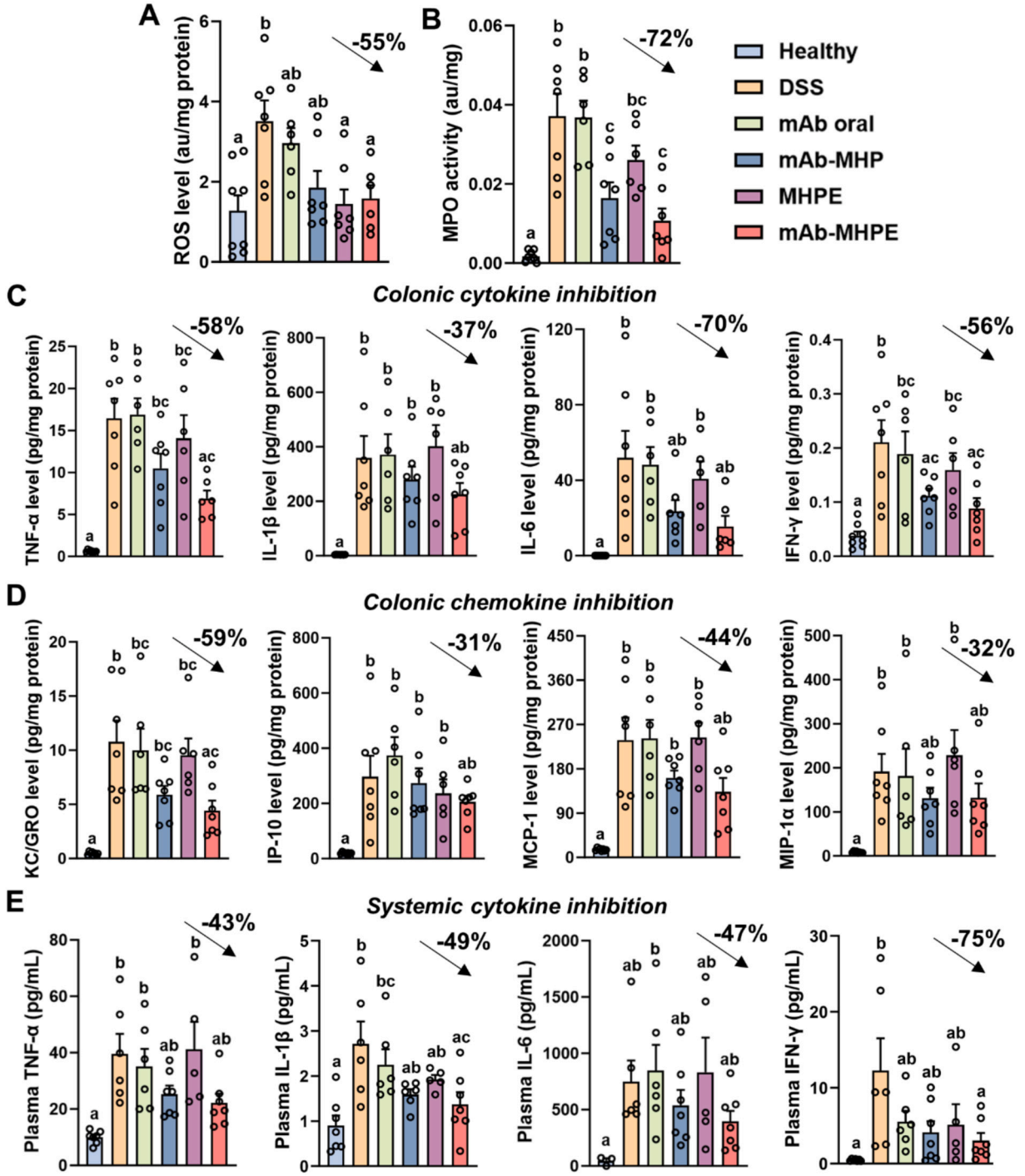

Fig. 8. Oral delivery of mAb-MHPE alleviated local and systemic inflammation in a DSS-induced chronic colitis model. (A) Colonic ROS levels and (B) MPO activity (mean ± SEM; n = 6–8). (C) Colonic levels of proinflammatory cytokines (TNF-α, IL-1β, IL-6, and IFN-γ) and (D) chemokines (KC/GRO, MCP-1, IP-10, and MIP-1α) were detected by ELISA after the indicated treatments (mean ± SEM; n = 6–8). (E) Plasma levels of proinflammatory cytokines (TNF-α, IL-1β, IL-6, and IFN-γ) were detected by ELISA after the indicated treatments (mean ± SEM; $n = 5$–8). Data with different superscript letters are significantly different ($^*p < 0.05$) according to one-way analysis of variance followed by Tukey's *post hoc* test. The black arrows represent the reduction in the oral mAb-MHPE group compared with the DSS group.

third cycles to better mimic the clinical practice of initiating therapy after symptom onset.

Compared with DSS group, mAb-MHPE treatment significantly reduced the colon weight/length ratio in mice (Fig. 7B), indicating its protective efficacy against DSS-induced colonic damage. A decrease in the histological score was observed in the mAb-MHPE group, but the score was not significantly different from that of the DSS group (Fig. 7C). mAb-MHPE treatment markedly reduced the endoscopic severity of colitis, as evidenced by a significant decrease in the MEICS score of 33 % (Fig. 7D). Strikingly, colonic ROS levels were significantly decreased in the mAb-MHPE-treated group (−55 % compared with those in the DSS group) to levels similar to those in healthy mice, demonstrating the antioxidative ability of mAb-MHPE (Fig. 8A). mAb-MHPE treatment also significantly lowered colonic MPO activity (−72 %) (Fig. 8B), indicating its capacity to mitigate neutrophil infiltration in the chronic colitis model. Strikingly, compared with the DSS group, mAb-MHPE treatment significantly reduced the colonic levels of proinflammatory cytokines, including TNF-α (−58 %) and IFN-γ (−56 %) (Fig. 8C), as well as the chemokine KC/GRO (−59 %) (Fig. 8D), highlighting its superior immunomodulatory efficacy. The levels of IL-1β (−37 %), IL-6 (−70 %), IP-10 (−31 %), MCP-1 (−44 %), and MIP-1α (−32 %) in the mAb-MHPE group were reduced to the same levels as those in the healthy group (Fig. 8C and D). In concrete, TNF-α levels in the mAb-MHPE group decreased to the same level as that in the healthy group (−58 % compared with the DSS group), whereas the mAb oral group showed no trend toward TNF-α reduction (+3 % compared with the DSS group) (Fig. 8C), indicating that mAb-MHPE successfully delivered the loaded mAb to the inflamed colon and effectively neutralized TNF-α.

Given that IBD is often associated with systemic manifestations, affecting up to 50 % of patients with at least one extraintestinal manifestation (EIM) [50], the systemic anti-inflammatory potential of mAb-MHPE was also explored. The pathophysiology of EIMs possibly involves the systemic extension of an immune-mediated response originating in the gut [50]. Therefore, we evaluated EIMs by analyzing plasma proinflammatory cytokine levels *via* ELISA (Mesoscale, USA). Compared with the DSS group, mAb-MHPE significantly decreased the plasma levels of IL-1β (−49 %) and IFN-γ (−75 %) and tended to reduce TNF-α (−43 %) and IL-6 levels (−47 %) in UC mice (Fig. 8E). These findings suggest that mAb-MHPE not only mitigated local colonic inflammation but also attenuated systemic inflammation, underscoring its potential to reduce systemic immune activation by controlling primary intestinal inflammation.

4. Conclusion

The oral delivery of antibodies, whose molecular weight can reach 150 kDa, remains a challenge because of degradation by the gastric acid and proteolysis, mucus clearance, and limited epithelial permeability [8]. We engineered antioxidant MOF nanoparticles with functional layers for effective oral colonic antibody delivery to address these issues, targeting different pathological pathways involved in IBD.

Previous studies for oral antibody delivery have mainly focused on lipid- or polymer-based nanocarriers for this purpose, particularly in IBD, given its chronic nature and the need for localized and sustained therapy [21–26,51]. While antioxidant MOFs have attracted attention for oral probiotic delivery due to their ability to protect cargo and scavenge ROS, their application in oral antibody delivery remained unexplored [52–54]. In this work, we leveraged these properties to design an antioxidant MOF with functional coatings that serves not only as a delivery vehicle for oral antibodies but also as a therapeutic agent, offering a novel approach to address IBD treatment.

Previous studies in oral antibody delivery for IBD treatment focused primarily on delivering infliximab [22–26]; however, the human constant region (accounting for 75 %) of infliximab can diminish efficacy and provoke immune responses in murine models [55]. Therefore, in this study, a murine TNF-α monoclonal antibody was integrated into a mAb-MOF with high encapsulation efficiency and noncompromised activity. The mAb-MOF was further functionalized with HA-PEG (mAb-MHP) to exploit mucus penetration and target inflammation. In two different acute murine colitis models, mAb-MHP demonstrated comparable or superior anti-inflammatory efficacy to intravenous mAb administration, whereas oral mAb solutions had no therapeutic effect. We further coated mAb-MHP with ES100 to develop a colon-targeting MOF nanosystem (mAb-MHPE). Its efficacy was assessed in murine models of acute and chronic colitis. mAb-MHPE significantly decreased oxidative stress, neutrophil infiltration, and the colonic levels of proinflammatory cytokines and chemokines. Notably, mAb-MHPE not only attenuated local colonic inflammation but also mitigated systemic inflammation in the chronic DSS model. Remarkably, in both acute and chronic colitis models, mAb-MHPE successfully alleviated the endoscopic severity of colitis, as assessed by colonoscopy, which is the gold standard for diagnosing remission in the clinic [3]. These findings underscore the consistent superior therapeutic effect of mAb-MHPE for IBD treatment.

While acute IBD models are widely used for rapid and cost-effective assessments of the immune response, they fail to capture chronic immune activation, which is central to IBD progression [37]. Our engineered anti-mouse TNF-α-loaded MOF exhibited robust and consistent therapeutic efficacy across multiple IBD models, including a chronic colitis model. In conclusion, the engineered antioxidative multifunctional MOF systems described in this work represent a step forward in the application of oral antibody delivery to achieve enhanced antibody delivery and effective local treatment.

Data and materials availability

All data supporting the results of this study are available within the paper and/or its Supplementary Information.

Declaration of generative AI and AI-assisted technologies in the writing process

During the preparation of this work the authors used ChatGPT in order to improve readability and language of the work. After using this tool/service, the authors reviewed the content and take full responsibility for the content of the publication.

CRediT authorship contribution statement

Cheng Chen: Writing – review & editing, Writing – original draft, Visualization, Methodology, Investigation, Formal analysis, Conceptualization. **Léo Guilbaud:** Investigation. **Valentina Marotti:** Investigation. **Wunan Zhang:** Investigation. **Inês Domingues:** Investigation. **Hafsa Yagoubi:** Investigation. **Katlijn Vints:** Methodology, Investigation. **Yining Xu:** Writing – review & editing, Writing – original draft, Visualization, Supervision, Resources, Project administration, Methodology, Investigation, Funding acquisition, Formal analysis, Conceptualization. **Ana Beloqui:** Writing – review & editing, Writing – original draft, Visualization, Supervision, Resources, Project administration, Methodology, Investigation, Funding acquisition, Formal analysis, Conceptualization.

Declaration of competing interest

Given her role as associate editor, Ana Beloqui had no involvement in the peer review of this article and had no access to information regarding its peer review. Full responsibility for the editorial process for this article was delegated to another journal editor. Ana Beloqui has served within the past 12 months as a consultant to Johnson & Johnson.

Acknowledgments

Cheng Chen is a PhD student at UCLouvain supported by the China Scholarship Council (CSC) and FRS-FNRS (Fonds de la Recherche Scientifique, Belgium). Yining Xu is a researcher funded by the National Natural Science Foundation of China Excellent Young Scholars Fund (Overseas) and General Program (82370860), the Department of Science and Technology of Sichuan Province (24YFHZ0326), the Fundamental Research Funds for the Central Universities (YJ202412) and 1.3.5 Project for Disciplines of Excellence (ZYYC25001). Ana Beloqui is a research associate from the FRS-FNRS and a WEL Research Institute investigator (WELBIO-CR-2022 S–01).

Appendix A. Supplementary data

Supplementary data to this article can be found online at https://doi.org/10.1016/j.jconrel.2025.114411.

Data availability

All data supporting the results of this study are available within the paper and/or its Supplementary Information.

References

[1] S. Liu, X. Wen, X. Zhang, S. Mao, Oral delivery of biomacromolecules by overcoming biological barriers in the gastrointestinal tract: an update, Expert Opin. Drug Deliv. 20 (2023) 1333–1347, https://doi.org/10.1080/17425247.2023.2231343.

[2] S. Alatab, S.G. Sepanlou, K. Ikuta, H. Vahedi, C. Bisignano, S. Safiri, A. Sadeghi, M. R. Nixon, A. Abdoli, H. Abolhassani, V. Alipour, The global, regional, and national burden of inflammatory bowel disease in 195 countries and territories, 1990-2017: a systematic analysis for the global burden of disease study 2017, Lancet, Gastroenterol. Hepatol. 5 (2020) 17–30, https://doi.org/10.1016/S2468-1253(19)30333-4.

[3] O.E. Okobi, I.O. Udoete, O.O. Fasehun, T. Okobi, E.O. Evbayekha, J.J. Ekabua, H. Elukeme, I.L. Ebong, O.O. Ajayi, I.V. Olateju, A. Taiwo, I.C. Anaya, J.A. Omole, M.B. Nkongho, U. Ojinnaka, A.O. Ajibowo, O.E. Ogbeifun, O.O. Ugbo, O. Okorare, Z. Akinsola, R.A. Olusoji, I.O. Amanze, J.N. Nwafor, N.A. Ukoha, T.A. Elimihele, A review of four practice guidelines of inflammatory bowel disease, Cureus 13 (2021) e16859, https://doi.org/10.7759/cureus.16859.

[4] A.G. Tamilarasan, G. Cunningham, P.M. Irving, M.A. Samaan, Recent advances in monoclonal antibody therapy in IBD: practical issues, Front. Gastroenterol. 10 (2019) 409–416, https://doi.org/10.1136/flgastro-2018-101054.

[5] G.J. Weiner, Building better monoclonal antibody-based therapeutics, Nat. Rev. Cancer 15 (2015) 361–370, https://doi.org/10.1038/nrc3930.

[6] T.T. Hansel, H. Kropshofer, T. Singer, J.A. Mitchell, A.J. George, The safety and side effects of monoclonal antibodies, Nat. Rev. Drug Discov. 9 (2010) 325–338, https://doi.org/10.1038/nrd3003.

[7] W. Zhang, C.B. Michalowski, A. Beloqui, Oral delivery of biologics in inflammatory bowel disease treatment, Front. Bioeng. Biotechnol. 9 (2021) 675194, https://doi.org/10.3389/fbioe.2021.675194.

[8] E. Moroz, S. Matoori, J.C. Leroux, Oral delivery of macromolecular drugs: where we are after almost 100years of attempts, Adv. Drug Deliv. Rev. 101 (2016) 108–121, https://doi.org/10.1016/j.addr.2016.01.010.

[9] T.D. Brown, K.A. Whitehead, S. Mitragotri, Materials for oral delivery of proteins and peptides, Nat. Rev. Mater. 5 (2019) 127–148, https://doi.org/10.1038/s41578-019-0156-6.

[10] C. Chen, A. Beloqui, Y. Xu, Oral nanomedicine biointeractions in the gastrointestinal tract in health and disease, Adv. Drug Deliv. Rev. 203 (2023) 115117, https://doi.org/10.1016/j.addr.2023.115117.

[11] H.S. de Souza, C. Fiocchi, Immunopathogenesis of IBD: current state of the art, Nat. Rev. Gastroenterol. Hepatol. 13 (2016) 13–27, https://doi.org/10.1038/nrgastro.2015.186.

[12] J.D. Feuerstein, K.L. Isaacs, Y. Schneider, S.M. Siddique, Y. Falck-Ytter, S. Singh, K. Chachu, L. Day, B. Lebwohl, T. Muniraj, A. Patel, AGA clinical practice guidelines on the management of moderate to severe ulcerative colitis, Gastroenterology 158 (2020) 1450–1461, https://doi.org/10.1053/j.gastro.2020.01.006.

[13] M.F. Neurath, Current and emerging therapeutic targets for IBD, Nat. Rev. Gastroenterol. Hepatol. 14 (2017) 269–278, https://doi.org/10.1038/nrgastro.2016.208.

[14] S. Li, F. Zhang, Q. Zhang, Pathological features-based targeted delivery strategies in IBD therapy: a mini review, Biomed. Pharmacother. 151 (2022) 113079, https://doi.org/10.1016/j.biopha.2022.113079.

[15] W. Fu, L. Xu, Z. Chen, L. Kan, Y. Ma, H. Qian, W. Wang, Recent advances on emerging nanomaterials for diagnosis and treatment of inflammatory bowel disease, J. Control. Release 363 (2023) 149–179, https://doi.org/10.1016/j.jconrel.2023.09.033.

[16] A. Awad, C.M. Madla, L.E. McCoubrey, F. Ferraro, F.K.H. Gavins, A. Buanz, S. Gaisford, M. Orlu, F. Siepmann, J. Siepmann, A.W. Basit, Clinical translation of advanced colonic drug delivery technologies, Adv. Drug Deliv. Rev. 181 (2022) 114076, https://doi.org/10.1016/j.addr.2021.114076.

[17] A. Michielan, R. D'Inca, Intestinal permeability in inflammatory bowel disease: pathogenesis, Clinical Evaluation, and Therapy of Leaky Gut, Mediat. Inflamm. 2015 (2015) 628157, https://doi.org/10.1155/2015/628157.

[18] M. Neurath, Current and emerging therapeutic targets for IBD, Nat. Rev. Gastroenterol. Hepatol. 14 (2017) 688, https://doi.org/10.1038/nrgastro.2017.138.

[19] Y. Xu, N. Shrestha, V. Preat, A. Beloqui, Overcoming the intestinal barrier: a look into targeting approaches for improved oral drug delivery systems, J. Control. Release 322 (2020) 486–508, https://doi.org/10.1016/j.jconrel.2020.04.006.

[20] W. Zhu, Y. Chao, Q. Jin, L. Chen, J.J. Shen, J. Zhu, Y. Chai, P. Lu, N. Yang, M. Chen, Y. Yang, Q. Chen, Z. Liu, Oral delivery of therapeutic antibodies with a transmucosal polymeric carrier, ACS Nano 17 (2023) 4373–4386, https://doi.org/10.1021/acsnano.2c09266.

[21] N. Shrestha, Y. Xu, J.R.C. Prevost, F. McCartney, D. Brayden, R. Frederick, A. Beloqui, V. Preat, Impact of PEGylation on an antibody-loaded nanoparticle-based drug delivery system for the treatment of inflammatory bowel disease, Acta Biomater. 140 (2022) 561–572, https://doi.org/10.1016/j.actbio.2021.12.015.

[22] L.J. Mohan, J.S. Daly, B.M. Ryan, Z. Ramtoola, Oral infliximab nanomedicines for targeted treatment of inflammatory bowel diseases, Eur. J. Pharm. Sci. 183 (2023) 106379, https://doi.org/10.1016/j.ejps.2023.106379.

[23] J.M. Kim, D.H. Kim, H.J. Park, H.W. Ma, I.S. Park, M. Son, S.Y. Ro, S. Hong, H. K. Han, S.J. Lim, S.W. Kim, J.H. Cheon, Nanocomposites-based targeted oral drug delivery systems with infliximab in a murine colitis model, J Nanobiotechnol. 18 (2020) 133, https://doi.org/10.1186/s12951-020-00693-4.

[24] X. Li, M. Yu, Z. Zhu, C. Lu, M. Jin, Y. Rao, Q. Zhao, X. Lu, C. Yu, Oral delivery of infliximab using nano-in-microparticles for the treatment of inflammatory bowel disease, Carbohydr. Polym. 273 (2021) 118556, https://doi.org/10.1016/j.carbpol.2021.118556.

[25] S.H. Lee, J.G. Song, H.K. Han, Site-selective oral delivery of therapeutic antibodies to the inflamed colon via a folic acid-grafted organic/inorganic hybrid nanocomposite system, Acta Pharm. Sin. B 12 (2022) 4249–4261, https://doi.org/10.1016/j.apsb.2022.06.006.

[26] X. Li, S. Fang, Y. Yu, H. Yang, Y. Rao, D. Hong, C. Lu, M. Yu, X. Lu, C. Yu, Q. Zhao, Oral administration of inflammatory microenvironment-responsive carrier-free infliximab nanocomplex for the targeted treatment of inflammatory bowel disease, Chem. Eng. J. 445 (2022), https://doi.org/10.1016/j.cej.2022.136438.

[27] A.A. Date, J. Hanes, L.M. Ensign, Nanoparticles for oral delivery: design, evaluation and state-of-the-art, J. Control. Release 240 (2016) 504–526, https://doi.org/10.1016/j.jconrel.2016.06.016.

[28] M. Ding, W. Liu, R. Gref, Nanoscale MOFs: from synthesis to drug delivery and theranostics applications, Adv. Drug Deliv. Rev. 190 (2022) 114496, https://doi.org/10.1016/j.addr.2022.114496.

[29] M. Kai, S. Wang, W. Gao, L. Zhang, Designs of metal-organic framework nanoparticles for protein delivery, J. Control. Release 361 (2023) 178–190, https://doi.org/10.1016/j.jconrel.2023.07.056.

[30] Q. Wang, C. Cheng, S. Zhao, Q. Liu, Y. Zhang, W. Liu, X. Zhao, H. Zhang, J. Pu, S. Zhang, H. Zhang, Y. Du, H. Wei, A valence-engineered self-cascading antioxidant nanozyme for the therapy of inflammatory bowel disease, Angew. Chem. Int. Ed. Eng. 61 (2022) e202201101, https://doi.org/10.1002/anie.202201101.

[31] J.T. Huckaby, S.K. Lai, PEGylation for enhancing nanoparticle diffusion in mucus, Adv. Drug Deliv. Rev. 124 (2018) 125–139, https://doi.org/10.1016/j.addr.2017.08.010.

[32] N.G. Kotla, S.R. Bonam, S. Rasala, J. Wankar, R.A. Bohara, J. Bayry, Y. Rochev, A. Pandit, Recent advances and prospects of hyaluronan as a multifunctional therapeutic system, J. Control. Release 336 (2021) 598–620, https://doi.org/10.1016/j.jconrel.2021.07.002.

[33] W.Y. Hernández, M.A. Centeno, S. Ivanova, P. Eloy, E.M. Gaigneaux, J. A. Odriozola, Cu-modified cryptomelane oxide as active catalyst for CO oxidation reactions, Appl. Catal. B Environ. 123-124 (2012) 27–35, https://doi.org/10.1016/j.apcatb.2012.04.024.

[34] W. Zhang, F. McCartney, Y. Xu, C.B. Michalowski, I. Domingues, E.K. Kambale, T. G. Moreels, L. Guilbaud, C. Chen, V. Marotti, D.J. Brayden, A. Beloqui, An in situ bioadhesive foam as a large intestinal delivery platform for antibody fragment to treat inflammatory bowel disease, J. Control. Release 374 (2024) 254–266, https://doi.org/10.1016/j.jconrel.2024.08.023.

[35] J.-M. Song, J.-H. Im, J.-H. Kang, D.-J. Kang, A simple method for hyaluronic acid quantification in culture broth, Carbohydr. Polym. 78 (2009) 633–634, https://doi.org/10.1016/j.carbpol.2009.04.033.

[36] G.E. Sims, T.J. Snape, A method for the estimation of polyethylene glycol in plasma protein fractions, Anal. Biochem. 107 (1980) 60–63, https://doi.org/10.1016/0003-2697(80)90492-3.

[37] S. Wirtz, V. Popp, M. Kindermann, K. Gerlach, B. Weigmann, S. Fichtner-Feigl, M. F. Neurath, Chemically induced mouse models of acute and chronic intestinal inflammation, Nat. Protoc. 12 (2017) 1295–1309, https://doi.org/10.1038/nprot.2017.044.

[38] C. Becker, M.C. Fantini, M.F. Neurath, High resolution colonoscopy in live mice, Nat. Protoc. 1 (2006) 2900–2904, https://doi.org/10.1038/nprot.2006.446.

[39] P.J. Koelink, M.E. Wildenberg, L.W. Stitt, B.G. Feagan, M. Koldijk, A.B. van t, R. Wout, M. Vieth Atreya, J.F. Brandse, S. Duijst, A.A. Te Velde, G. D'Haens, B. G. Levesque, G.R. van den Brink, Development of reliable, valid and responsive

scoring Systems for Endoscopy and Histology in animal models for inflammatory bowel disease, J. Crohns Colitis 12 (2018) 794–803, https://doi.org/10.1093/ecco-jcc/jjy035.
[40] N. Hanning, J.G. De Man, B.Y. De Winter, Measuring myeloperoxidase activity as a marker of inflammation in gut tissue samples of mice and rat, Bio-Protoc. 13 (2023) e4758, https://doi.org/10.21769/BioProtoc.4758.
[41] A. Huguet-Casquero, Y. Xu, E. Gainza, J.L. Pedraz, A. Beloqui, Oral delivery of oleuropein-loaded lipid nanocarriers alleviates inflammation and oxidative stress in acute colitis, Int. J. Pharm. 586 (2020) 119515, https://doi.org/10.1016/j.ijpharm.2020.119515.
[42] E. Viennois, F. Chen, H. Laroui, M.T. Baker, D. Merlin, Dextran sodium sulfate inhibits the activities of both polymerase and reverse transcriptase: lithium chloride purification, a rapid and efficient technique to purify RNA, BMC. Res. Notes 6 (2013) 360, https://doi.org/10.1186/1756-0500-6-360.
[43] M. Alhouayek, B. Buisseret, A. Paquot, O. Guillemot-Legris, G.G. Muccioli, The endogenous bioactive lipid prostaglandin D(2)-glycerol ester reduces murine colitis via DP1 and PPARgamma receptors, FASEB J. 32 (2018) 5000–5011, https://doi.org/10.1096/fj.201701205R.
[44] K. Liang, R. Ricco, C.M. Doherty, M.J. Styles, S. Bell, N. Kirby, S. Mudie, D. Haylock, A.J. Hill, C.J. Doonan, P. Falcaro, Biomimetic mineralization of metal-organic frameworks as protective coatings for biomacromolecules, Nat. Commun. 6 (2015) 7240, https://doi.org/10.1038/ncomms8240.
[45] I.S. Bayer, Recent advances in mucoadhesive Interface materials, Mucoadhesion characterization, and technologies, Adv. Mater. Interfaces 9 (2022), https://doi.org/10.1002/admi.202200211.
[46] M.F. Neurath, Cytokines in inflammatory bowel disease, Nat. Rev. Immunol. 14 (2014) 329–342, https://doi.org/10.1038/nri3661.
[47] A. Viola, G. Costantino, A.C. Privitera, F. Bossa, A. Lauria, L. Grossi, M.B. Principi, N. Della Valle, M. Cappello, Clinical and economic impact of infliximab one-hour infusion protocol in patients with inflammatory bowel diseases: a multicenter study, world J Gastrointest, Pharmacol. Ther. 8 (2017) 131–136, https://doi.org/10.4292/wjgpt.v8.i2.131.
[48] V. Marotti, Y. Xu, C. Bohns Michalowski, W. Zhang, I. Domingues, H. Ameraoui, T. G. Moreels, P. Baatsen, M. Van Hul, G.G. Muccioli, P.D. Cani, M. Alhouayek, A. Malfanti, A. Beloqui, A nanoparticle platform for combined mucosal healing and immunomodulation in inflammatory bowel disease treatment, Bioact Mater 32 (2024) 206–221, https://doi.org/10.1016/j.bioactmat.2023.09.014.
[49] V. Annese, M. Daperno, M.D. Rutter, A. Amiot, P. Bossuyt, J. East, M. Ferrante, M. Gotz, K.H. Katsanos, R. Kiesslich, I. Ordas, A. Repici, B. Rosa, S. Sebastian, T. Kucharzik, R. Eliakim, C.S. European, O. Colitis, European evidence based consensus for endoscopy in inflammatory bowel disease, J Crohns Colitis 7 (2013) 982–1018, https://doi.org/10.1016/j.crohns.2013.09.016.
[50] S.R. Vavricka, A. Schoepfer, M. Scharl, P.L. Lakatos, A. Navarini, G. Rogler, Extraintestinal manifestations of inflammatory bowel disease, Inflamm. Bowel Dis. 21 (2015) 1982–1992, https://doi.org/10.1097/MIB.0000000000000392.
[51] X. Wang, J. Yan, L. Wang, D. Pan, Y. Xu, F. Wang, J. Sheng, X. Li, M. Yang, Oral delivery of anti-TNF antibody shielded by natural polyphenol-mediated supramolecular assembly for inflammatory bowel disease therapy, Theranostics 10 (2020) 10808–10822, https://doi.org/10.7150/thno.47601.
[52] L. Zhu, T. Yu, W. Wang, T. Xu, W. Geng, N. Li, X. Zan, Responsively degradable Nanoarmor-assisted super resistance and stable colonization of probiotics for enhanced inflammation-targeted delivery, Adv. Mater. 36 (2024) e2308728, https://doi.org/10.1002/adma.202308728.
[53] F. Cao, L. Jin, Y. Gao, Y. Ding, H. Wen, Z. Qian, C. Zhang, L. Hong, H. Yang, J. Zhang, Z. Tong, W. Wang, X. Chen, Z. Mao, Artificial-enzymes-armed Bifidobacterium longum probiotics for alleviating intestinal inflammation and microbiota dysbiosis, Nat. Nanotechnol. 18 (2023) 617–627, https://doi.org/10.1038/s41565-023-01346-x.
[54] J. Zhou, M. Li, Q. Chen, X. Li, L. Chen, Z. Dong, W. Zhu, Y. Yang, Z. Liu, Q. Chen, Programmable probiotics modulate inflammation and gut microbiota for inflammatory bowel disease treatment after effective oral delivery, Nat. Commun. 13 (2022) 3432, https://doi.org/10.1038/s41467-022-31171-0.
[55] M.B. Assas, S.E. Levison, M. Little, H. England, L. Battrick, J. Bagnall, J. T. McLaughlin, P. Paszek, K.J. Else, J.L. Pennock, Anti-inflammatory effects of infliximab in mice are independent of tumour necrosis factor alpha neutralization, Clin. Exp. Immunol. 187 (2017) 225–233, https://doi.org/10.1111/cei.12872.